4-13-2019

Deletion of *ULS1* Confers Damage Tolerance in sgs1 Mutants Through a Top3-dependent D-loop Mediated Fork Restart Pathway

M. Rebecca Glineburg

Eleanor Johns

F. Brad Johnson

Deletion of *ULS1* Confers Damage Tolerance in sgs1 Mutants Through a Top3-dependent D-loop Mediated Fork Restart Pathway

Deletion of *ULS1* confers damage tolerance in *sgs1* mutants through a Top3-dependent D-loop mediated fork restart pathway

M. Rebecca Glineburg[a,b,I], Eleanor Johns[a], and F. Brad Johnson[a,b,c,II,]

From the [a]*Department of Pathology and Laboratory Medicine,* [b]*Cell and Molecular Biology Group, Biomedical Graduate Studies, and the* [c]*Institute of Aging, University of Pennsylvania School of Medicine, Philadelphia, Pennsylvania 19104*

[I]*Current Address: Neurology Department, University of Michigan, Ann Arbor, Michigan 48109*

[II]To whom correspondence should be addressed at:

405A Stellar Chance Labs
422 Curie Blvd
Philadelphia, PA 19106
johnsonb@pennmedicine.upenn.edu

Abstract

Homologous recombination (HR)-based repair during DNA replication can apparently utilize several partially overlapping repair pathways in response to any given lesion. A key player in HR repair is the Sgs1-Top3-Rmi1 (STR) complex, which is critical for resolving X-shaped recombination intermediates formed following bypass of methyl methanesulfonate (MMS)-induced damage. STR mutants are also sensitive to the ribonucleotide reductase inhibitor, hydroxyurea (HU), but unlike MMS treatment, HU treatment is not accompanied by X-structure accumulation, and it is thus unclear how STR functions in this context. Here we provide evidence that HU-induced fork stalling enlists Top3 prior to recombination intermediate formation. The resistance of *sgs1Δ* mutants to HU is enhanced by the absence of the putative SUMO (Small Ubiquitin MOdifier)-targeted ubiquitin ligase, Uls1, and we demonstrate that Top3 is required for this enhanced resistance and for coordinated breaks and subsequent D-loop formation at forks stalled at the ribosomal DNA (rDNA) replication fork block (RFB). We also find that HU resistance depends on the catalytic activity of the E3 SUMO ligase, Mms21, and includes a rapid Rad51-dependent restart mechanism that is different from the slow Rad51-independent HR fork restart mechanism operative in *sgs1Δ ULS1+* mutants. These data support a model in which repair of HU-induced damage in *sgs1Δ* mutants involves an error-prone break-induced replication pathway but, in the absence of Uls1, shifts to one that is higher-fidelity and involves the formation of Rad51-dependent D-loops.

Highlights

- The Top3 topoisomerase is required for the HU resistance conferred to *sgs1Δ* mutants by deletion of the putative SUMO-targeted ubiquitin ligase, Uls1.
- Top3 is required for coordinated breaks and D-loop formation within the rDNA following HU-induced damage.
- Absence of Uls1 channels repair of HU-induced damage in *sgs1Δ* mutants from a Rad51-independent HR pathway to a Rad51-dependent HR pathway.
- Rescue of *sgs1Δ* mutants by deletion of *ULS1* requires the SUMO ligase activity of Mms21.

Keywords

Top3, Uls1, homologous recombination, D-loop, hydroxyurea, rDNA

Introduction

Maintaining genome integrity is vital for cell survival and cancer prevention. This maintenance is particularly challenging in the context of replication, where DNA repair machinery must coordinate activities with the replisome. It is well established that cells have a number of partially overlapping pathways that can repair DNA damage during replication, but how pathway choice is decided is still unclear. Recently, it has become evident that an intricate crosstalk occurring between the replication machinery, chromatin structure, and DNA repair complexes can strongly influence repair pathway choice (Reviewed in [1, 2]). A better understanding of how these different pathways assist and compensate for one another to repair a given lesion could provide insight into cancer chemotherapeutic strategies.

The ribonucleotide reductase inhibitor, hydroxyurea (HU) predominantly induces replication fork stalling, causing uncoupling of the replicative MCM helicase from the polymerase machinery and generating ssDNA ahead of replicated DNA; in some DNA repair mutant backgrounds this stalling can further lead to reversal of the replication fork [3-7]. Interestingly, while fork reversal with subsequent fork restart is one of the primary responses to fork stalling in mammalian cells, likely due to the action of PARP, it is a rare event in yeast; fork restart in yeast thus must arise by other mechanisms [8-11].

The STR complex, comprising the RecQ helicase Sgs1, the topoisomerase Top3, and the OB-fold containing protein Rmi1, is critical for genome integrity, including the HR-dependent reestablishment of damaged replication forks. Mutations in any of the STR complex members lead to increased rates of aberrant recombination, and elevated levels of X-shaped recombination intermediates during S-phase, particularly in the setting of MMS-induced DNA damage [12-17]. Both *in vitro* and *in vivo* studies strongly indicate a direct role for this complex in resolving

recombination intermediates, through the combined catalytic activities of the Sgs1 helicase unwinding DNA and the Top3 topoisomerase transiently nicking and mediating strand passage to decatenate joint molecules [13-15, 18-20]. Previous work from our own lab has shown *sgs1Δ top3Δ* mutants are more sensitive than *sgs1Δ* mutants to MMS, and that Top3 is capable of working independently from its complex members to resolve a specific type of MMS-induced X-shaped and hemicatenated template switch recombination intermediate termed a Rec-X [13].

However, *STR* mutants are similarly sensitive to HU, which unlike MMS, does not result in X-structure accumulation, indicating that the STR complex could have important functions outside of X-shaped recombination intermediate resolution [12, 15]. Indeed, Sgs1 has also been implicated in earlier steps in the rescue of damaged forks including polymerase stabilization, Rad53 DNA damage response kinase recruitment, and 5' DNA end resection, with Top3 and Rmi1 serving primarily to support Sgs1 in these contexts [21-25]. These functions likely aid in fork stabilization, but whether other functions of the STR complex are important at the fork and whether Top3 is capable of additional independent roles outside of Rec-X resolution are not fully understood. Interestingly, deletion of *SGS1* results in increased rates of break-induced replication (BIR) and a compensatory loss of gene conversion (GC) events (*i.e.* synthesis dependent strand annealing and double Holliday junction (dHJ)-mediated HR events) following a double strand break (DSB), suggesting Sgs1, and possibly other STR complex members can mediate repair pathway choice in this setting [26, 27]. However, how these activities might influence repair pathway choice at damaged replication forks has not been explored.

Recently it has been shown that genetic inactivation Uls1, a Swi2/Snf2-related putative SUMO-targeted ubiquitin ligase (STUbL), provides damage tolerance to *sgs1Δ* mutants in a post-replicative, HR-dependent manner [28, 29]. Given our previous observations that

overexpression of Top3 can also provide rescue to *sgs1Δ* mutants on MMS, we investigated whether the rescue conferred by deletion of *ULS1* required these same Top3 functions. We find that rescue of *sgs1Δ* mutants in the absence of Uls1, while dependent on Top3, does not involve Top3-mediated Rec-X resolution but instead utilizes a novel Top3-mediated break-induced fork restart mechanism. Furthermore, we provide evidence that repair of HU-induced stalled forks occurs predominantly through D-loop intermediates to restart replication, and that deletion of *ULS1* confers resistance in *sgs1Δ* mutants by shifting this D-loop mediated repair from a Rad51-independent to a Rad51-dependent pathway.

Experimental Procedures

Yeast strains and plasmids

All yeast strains used were derived from the BY4741/2 background, with the exception of the HO-inducible crossover assay strains (derived from JMK background strains gifted by Jim Haber). *bar1Δ* strains were used for all synchronization assays. Table 1 provides a list of all strains used.

Spot assays: Fresh yeast cultures, grown overnight at 23°C (and under selective conditions for strains carrying plasmids), were spotted in 10-fold serial dilutions on YPAD or YPAD + drug plates as previously described [13]. Experiments were performed at 30°C, and images were taken at 48 hrs unless otherwise indicated. At least 3 independent experiments were conducted for each spot assay.

*Analysis of recombination intermediates via 2D-gel electrophoresis & Southern blotting (*2DGE-SB)*:* Preparation of cell cultures, DNA purification, and 2DGE-SB for analyzing the rDNA,

region adjacent to ARS305 was performed as previously described [13, 30]. Cells were synchronized in G1 with α-factor for 4 hours, released into fresh YPAD containing 200 mM HU and allowed to grow for 1 hr. At this time, cells were either harvested, or spun down and resuspended in fresh YPAD containing no drug and grown for the times indicated prior to harvest. For experiments utilizing *in vivo* crosslinking, cells were grown and harvested as above. At the time of harvest, cells were resuspended in 5 mL cold dH_2O at 4 $x10^8$ cells/mL and UV crosslinked 5 times with 300 µL of 200 µg/ml psoralen in EtOH for 5 min, with 5 min incubations on ice between rounds of crosslinking, as described [31] Branch migration assays were performed after the first dimension at 65°C for 6 hrs as described [30]. Mung bean nuclease (MBN) assays were performed using 45 units per 5 µg of DNA as described [13, 30]. 2 to 3 independent experiments, each with 2 to 3 replicates for each genotype were performed for all 2DGE-SB experiments, and samples within each experiment were run in parallel to account for variation in gel preparation. Gels were quantified using Imagequant analyses of Phosphorimager scans. *P*-values for X-spike:small arc and (large arc + RFB):small arc ratios were calculated using two-tailed Student's t-tests.

Morphology assays: Cells were grown as described above for 2DGE-SB, collected and counted at the specified time points. Additional samples at each timepoint were fixed dropwise with 70% ethanol and micrographs were obtained the following day. We note that extended exposure to α-factor can influence cell morphology, and so an additional wash of the cells with fresh YPAD prior to exposure to HU was performed to eliminate all traces of α-factor. Cells were counted as aberrant if they presented as a cluster of three or more intact cells. Each cluster was counted as one cell. Cells were photographed on the bright field setting at 40X magnification and using Olympus DP software. *P*-values for 12 hour recovery (Figure 2A) were calculated using

Fisher's exact test. >350 cells were counted for each genotype. *P-values* for Figure 2B & C were calculated using one-way ANOVAs.

Viability following acute HU exposure assay: Cells were grown as described for morphology assays, followed by a 6 hr recovery in YPAD. Cells were then sonicated with a cup horn at 90% energy for 1 min, counted, and 1000 cells were plated on YPAD. This level of sonication did not affect cell viability in control experiments, but was sufficient to disrupt residual filamentous cell clusters. Colony-forming units (CFUs) were counted after 3 days, and the percentage of cells plated forming colonies calculated. P-values for Figure 2D were calculated using two-tailed, unpaired Student's T-test.

rDNA break assay: Cells were grown as described above for 2DGE-SB experiments, in 5 ml volumes. Plug preparation, digest, running conditions, and Southern blotting for the rDNA break assay has been described previously [32]. In brief, cells were imbedded into agarose plugs with zymolyase and digested in a 6 well plate sequentially: 2X zymolyase at 37^0C for 24 hrs, 2X 1 mg/ml proteinase K and 2.5% sarkosyl at 50^0C for 24 hrs, 1X 40 µg/ml PMSF for 1 hr, washed with TE 1hr at 50^0C, 1X 100 µg/ml RNase A, at 50^0C for 3 hrs, and digested with Bgl II overnight at 37^0C. Plugs were washed with TE prior to loading on a 1% agarose gel in 1X TBE. ER5A-up, 5′-GCC ATT TAC AAA AAC ATA ACG-3′ and ER5A-lower, 5′-GGG CCT AGT TTA GAG AGA AGT-3′ were used to make Probe A *via* PCR amplification of genomic DNA [32]. Breaks were quantified using Imagequant analyses of Phosphorimager scans. The proportion of breaks was determined by dividing the intensity of the 2.3 Kb band by that of the 4.6 Kb band. Quantification for two individual colonies for each genotype are shown.

Crossover assays: The *ADE2* crossover assay, and the HO-inducible crossover assay, have been previously described [13, 16, 33]. *P*-values for comparing *sgs1Δ* to *sgs1Δ uls1Δ* were quantified using two-tailed Student's t-tests for the *ADE2* crossover assay and for the 6 hr time point for the HO-inducible crossover assay. Fisher's exact test was used to calculate *p*-values for comparing *sgs1Δ* and *sgs1Δ uls1Δ* differences in the single colony analysis. At least 149 colonies were analyzed for each genotype.

Results

Rescue of *sgs1Δ* by deletion of *ULS1* is dependent on Top3

Inactivation of Uls1 has previously been shown to provide rescue to *sgs1Δ* mutants on MMS and HU, in a HR-dependent manner [28, 29]. Furthermore, this rescue *via* deletion of *ULS1* appeared to be specific for *sgs1Δ* mutants, as deletion of *ULS1* was unable to provide rescue to *top3Δ* and *rmi1Δ* mutants [28, 29]. Although it normally functions at least in part within the full STR complex, Top3 is capable of working independently from its complex members to provide rescue on MMS in a HR-dependent manner, and so we investigated the possibility that the rescue of *sgs1Δ* mutants observed with *ULS1* deletion requires Top3 [13]. To address this, we first confirmed that deletion of *ULS1* does indeed confer damage tolerance to *sgs1Δ* mutants exposed to DNA damaging agents and that it does not provide such tolerance to WT cells in our strain background (Figure 1A; of note, rescue was weak on MMS, but more substantial on HU. See the next paragraph). However, deletion of *ULS1* failed to rescue the growth of *sgs1Δ top3Δ* mutants on MMS or HU indicating that Top3 is required for the damage tolerance observed when *ULS1* is deleted in *sgs1Δ* mutants (Figure 1A). Consistent with our previous findings [13], rescue of *sgs1Δ* mutants by deletion of *ULS1* is independent of Rmi1,

indicating a role for Top3 that is independent of the STR complex. Rescue of *sgs1Δ* mutants by deletion of *ULS1* also requires Top3 catalytic activity, as expression of the catalytically dead *top3-Y356F* mutant did not provide rescue on HU to *sgs1Δ top3Δ uls1Δ* mutants (Figure 1B). Furthermore, when Top3 was overexpressed (OE) in *sgs1Δ uls1Δ* mutants, there was a small, but reproducible, increase in HU tolerance compared to *sgs1Δ uls1Δ* mutants, or to *sgs1Δ* mutants with Top3 OE, indicating Top3 levels are limiting for HU resistance in the absence of Uls1 (Figure 1C).

As noted above, the rescue observed by deletion of *ULS1* in *sgs1Δ* mutants was consistently more prominent in the presence of HU than MMS. This, together with the lack of X-structure accumulation in HU-treated cells [12], led us to hypothesize that in the absence of Uls1, Top3 functions independently of its known X-structure resolution activity to provide rescue to *sgs1Δ* mutants on HU. We thus chose to focus our investigation on how Top3 confers tolerance to HU-induced damage in *sgs1Δ* mutants lacking Uls1.

Rescue of *sgs1Δ* mutants by deletion of *ULS1* is through an accelerated Top3-dependent DNA repair mechanism

Deletion of *ULS1* could promote recovery from HU via two different mechanisms: 1) increasing the speed of recovery or 2) preventing cell death. For example, the first type of mechanism could involve faster recovery from checkpoint arrest perhaps due to selection of a faster repair pathway, whereas the second could involve avoidance of a repair pathway leading to intermediates that are toxic in the absence of Sgs1. To distinguish between these possibilities, and to determine what role Top3 provides in this context, we performed the following experiments.

In normal *S. cerevisiae* cells, HU treatment induces filamentous growth, characterized by elongated cells that remain linked to one another in pseudohyphal structures [34]. This occurs in a fashion dependent on the Mec1 and Rad53 DNA damage checkpoint kinases and is reversible following release from HU [34]. We wondered whether the Top3-dependent damage tolerance conferred by deletion of *ULS1* in *sgs1Δ* mutants affected filamentous growth. Cells were synchronized in G1 with α-factor, released into 200 mM HU for one hour, and monitored during recovery. We observed a statistically significant decrease in the percentage of cells with filamentous morphology—defined as clusters of three or more interlinked cells—in *sgs1Δ uls1Δ* compared to *sgs1Δ* mutants following 12 hours of recovery from HU, whereas no difference was observed between *sgs1Δ, sgs1Δ top3Δ* and *sgs1Δ top3Δ uls1Δ* mutants (Figure 2A). These observations support a role for Top3 in alleviating HU-induced filamentous growth of cells lacking Sgs1 and Uls1.

We next examined whether Top3 in *sgs1Δ uls1Δ* mutants inhibits the induction of filamentous growth or instead promotes faster resolution of events leading to filamentous growth. To this end, we followed the progression of cell morphology over time in *sgs1Δ*, *sgs1Δ uls1Δ, sgs1Δ top3Δ,* and *sgs1Δ top3Δ uls1Δ* cells following recovery from HU exposure. In steady state growth, all four genotypes accumulated an elevated population of large budded cells, as if in apparent G2/M, typical of DNA repair mutants. However, the majority of these cells responded to α-factor, indicating passage through G1, as evidenced by the large number of "shmoo doublets" (*i.e.* linked mother and daughter cells displaying morphological responses to α-factor; Supplemental Figure 1, *arrows*). We found that all genotypes examined entered S-phase in the presence of HU at similar rates, as determined by bud morphology, and accumulated equivalent levels of filamentous growth, which persisted up until 3 hours following recovery,

with minimal increases in cell number. Together, this suggests Top3 and deletion of *ULS1* do not prevent filamentous growth in *sgs1Δ* mutants (Figure 2B-2C and Supplemental Figure 1). However, at 4.5 hours following release from HU, we observed a sudden decrease in the number of filamentous cells in all cell types, with the most dramatic decrease (~two-fold) occurring for *sgs1Δ uls1Δ* (Figure 2B and Supplemental Figure 1). These decreases correlated with an equivalent increase in cell number, again with *sgs1Δ uls1Δ* mutants having the most dramatic (>two-fold) increase in cell number (Figure 2C). Importantly, these observations place the activity of Top3 downstream of HU-induced fork stalling, and support a model in which deletion of *ULS1* promotes faster recovery from damage via a Top3-dependent process, rather than affecting an earlier stage by preventing damage.

To determine whether deletion of *ULS1* and Top3 have a role in cell viability, we treated synchronized cells with HU, followed by 6 hours of recovery. Cells were then sonicated gently to disrupt any remaining filamentous structures, and equivalent cell numbers were plated on YPAD. *sgs1Δ uls1Δ* had a significant increase in colony-forming unit (CFU) efficiency compared to *sgs1Δ* mutants; however, this increase was not entirely dependent on Top3, as *sgs1Δ top3Δ uls1Δ* mutants also had significantly higher CFU efficiency compared to *sgs1Δ top3Δ* mutants (Figure 2D). Together, these results suggest that deletion of *ULS1* confers resistance to *sgs1* mutants acutely exposed to HU by two mechanisms: 1) accelerating repair *via* a Top3-dependent process, and 2) promoting viability *via* a Top3-independent process. Given the requirement for Top3 to provide rescue to *sgs1Δ uls1Δ* mutants chronically exposed to HU (Figure 1A), we suspect this first mechanism is the primary means by which deletion of *ULS1* confers HU resistance to *sgs1Δ* mutants.

Rescue of *sgs1Δ* mutants by deletion of *ULS1* is accompanied by Top3-mediated fork restart

Given the dependence of DNA replication stress-induced filamentous growth on Rad53, we speculated that the HU-induced pseudohyphal phenotype could be due to cells entering mitosis without completing replication and/or without resolving DNA linkages formed during HR. Previous work has implicated Uls1 activity occurring upstream of recombination intermediate formation [28, 29]; however, it has been well established that Top3 has roles downstream of recombination intermediate formation [13-15, 35]. Because deletion of *ULS1* causes more rapid resolution of filamentous morphology during recovery from HU (Figure 2 and Supplemental Figure 1) we considered the possibility that this might reflect faster resolution of replication-associated recombination intermediates. We investigated this using two-dimensional gel electrophoresis and Southern blotting (2DGE-SB) to observe potential recombination intermediates formed in the presence of, and following recovery from, HU. We found no differences in X-structure levels in *sgsΔ vs sgs1Δ uls1Δ* mutants within the rDNA on a fragment containing the RFB or at a fragment adjacent to *ARS305* (Figure 3A; Supplemental Figure 2A, and 2B respectively). These findings are consistent with previous observations of cells exposed to MMS [29]. However, there was a small, yet reproducible HU-induced increase (1.2-fold) in RFB and large fork structures in the *sgs1Δ uls1Δ* mutants *vs sgs1Δ* mutants detected within the rDNA fragment (*i.e.* structures migrating together with Y-shaped replication intermediates at or larger than those at the RFB; Figures 3A-3B, 4C, and data not shown). Because deletion of *ULS1* could be stabilizing X-structures, which might resolve spontaneously by branch migration during sample preparation and thus be difficult to detect, we also used psoralen crosslinking of cells to stabilize DNA structures prior to their isolation. Again, X-structure levels were

unchanged, but we observed an even larger and significant increase (1.4 fold) in RFB and large arc structures in *sgs1Δ uls1Δ* mutants compared to *sgs1Δ* mutants, suggesting that these structures are unstable (Figure 3C). Intriguingly, this increase in large fork structures, which we initially interpreted as fork stalling, partially required Top3 activity, as *sgs1Δ uls1Δ top3Δ* mutants consistently had significantly reduced levels of large forks compared to *sgs1Δ uls1Δ* mutants (Figure 3D). Furthermore, we saw no increase in large fork structures when we compared *sgs1Δ top3Δ* and *sgs1Δ uls1Δ top3Δ* mutants (Supplemental Figure 2C). These observations led us to hypothesize that Top3, instead of having its traditional roles in X-structure resolution, functions prior to X-structure formation, perhaps to stabilize stalled forks.

To determine if Top3 was helping to stabilize forks in the absence of Uls1, we measured breaks at the rDNA RFB in cells exposed to HU using a published assay [32]. In brief, DNA was digested to produce rDNA fragments of 4.6 Kb in length with ~2.3 Kb of sequence on either side of the RFB (Figure 3E). Distinct bands of 2.3 and 2.2 Kb are visualized in this system, indicative of broken forks stalled at the RFB [32]. To our surprise, we observed not a decrease, but an increase in RFB-specific breaks in *sgs1Δ uls1Δ* mutants compared to *sgs1Δ* mutants, and this increase in breaks required Top3 (Figure 3E-3F). Because breaks during S-phase are predominantly repaired *via* HR mechanisms, and because HR is required for *uls1Δ*-mediated rescue of *sgs1Δ* mutants, we wondered if the species migrating on the large arc in 2DGE might be related to HR-mediated repair of the RFB breaks.

Rescue of *sgs1* mutants by deletion of *ULS1* is correlated with HR-mediated fork restart

To gain insight into the structures of the large arc species, samples were incubated between the first and second dimensions of 2DGE under conditions where certain recombination

intermediates can branch migrate and thus resolve into new structures (Figure 4A-4B) [12, 30, 36]. The effect of Mg^{2+} was examined because it can inhibit the migration of various types of branched DNA structures to different degrees. In particular, HJs and reversed forks can branch migrate in the absence of Mg^{2+}, but form antiparallel stacked-X structures which impede branch migration in the presence of Mg^{2+} [36]. In contrast, hemicatenanes and Rec-Xs are able to branch migrate to similar degrees with or without Mg^{2+}, but because these run as X-structures they should not explain the large arc structures we observe [30]. Although stalled forks *per se* would not branch migrate at all, under our branch migration conditions stalled forks might regress spontaneously, enabling further branch migration, but only when Mg^{2+} is absent because regressed forks are topologically equivalent to HJs (Supplemental Figure 3A). When DNA species from HU-treated *sgs1Δ* or *sgs1Δ uls1Δ* cells were allowed to branch migrate between the first and second dimensions of 2DGE, large arc species were converted into several novel products (spots a, b, and c, and the cone above and to the left of the Y-arc in Figure 4A-B), and the conversion was actually enhanced, not inhibited, by Mg^{2+}. The findings suggest that some species migrating with the RFB and large arc are D-loops, as follows. First, D-loops exist in an open conformation, which cannot isomerize into a stacked X configuration, making them resistant to Mg^{2+} entrapment. Second, sister chromatids entwined by a D-loop are topologically similar to chromatids held together by a replication fork (Figure 4B, *top*, species *iv* and *v vs. iii*), and indeed have been shown previously to migrate along the replication arc in 2DGE [37]. Third, two sets of products were generated by branch migration, having either increased (spots a, b, & c) or decreased (cone above and left of the Y-arc) mobility in the second dimension when compared with the large arc species from which they are derived (Figure 4A, *bottom panels*). The mobilities of the products can be explained, as follows, by a population of branch migrating

D-loops, each formed *in vivo* from a broken fork at the RFB followed by invasion of the truncated chromatid into its intact sister chromatid, and extended to varying extents by new DNA synthesis and migration of the D-loop (Figure 4B, *top*, species *ii*, *iv* and *v*). In the case of a D-loop formed between the intact (*vii*) and truncated (*viii*) chromatid arms, but prior to the initiation of DNA synthesis, branch migration to immediately separate the chromatids (*i.e.* migration to the right in Figure 4B) would result in the two distinct high mobility products indicated as spots *b* and *c*. In other words, while the chromatids engaged in the D-loop migrate in the first dimension in the same fashion as forks stalled at the RFB, when separated by branch migration they run as full length and truncated fragments in the second dimension, whereas stalled forks resist branch migration and remain on the Y-arc. Spot *a* corresponds to a D-loop that has been fully extended by DNA synthesis to the end of the fragment, and then separated by branch migration into two full-length duplex fragments. The line connecting spots *c* and *a* (*ix*) contains D-loops extended by DNA synthesis to varying extents such that the size in the second dimension decreases in proportion to how far synthesis has progressed along the large half of the replication arc. In contrast, the structures generated by branch migration in the other direction (*i.e.* to the left in Figure 4B, species *vi*) are bulkier than D-loops/replication forks and thus run in a cone-shaped area to the left and above of the large arc (Figure 4B). Reversed forks have also been shown to migrate within this cone; however as noted above, resolution into linear fragments should be impeded by Mg^{2+} (Supplemental Figure 3A) [3]. Thus, the new species generated by branch migration cannot be explained by HJ, reversed fork, or hemicatenated intermediates, but are consistent with the D-loop model, although we cannot rule out the possibility that DNA structures other than those we have considered might be involved.

To further characterize the large arc species, we treated our samples with the single strand specific nuclease, mung bean nuclease (MBN). D-loops have regions of single stranded DNA and should be sensitive to MBN, which would digest the displaced strand in a D-loop, resulting in structures resembling nicked fork structures, while reversed forks should be resistant. Indeed, large arc-structures in *sgs1Δ* mutants exposed to HU are sensitive to MBN, as seen by an overall reduction in the large arc signal following treatment with MBN (Supplemental Figure 3B). Importantly, we do not see a reduction in X-structure levels following MBN treatment, suggesting these could be HJ-shaped structures and thus act as internal controls for MBN specificity in our assay.

We next sought to determine whether the apparent D-loops arose from the same or different HR repair pathways. While effectively all HR repair pathways require Rad52, Rad51 is required only for GC and some forms of template switching, and is dispensable for single-strand annealing (SSA) and some forms of BIR [38-41]. We compared HU-induced replication intermediates in *sgs1Δ* and *sgs1Δ uls1Δ* strains to HU-induced replication intermediates in *sgs1Δ rad51Δ* and *sgs1Δ uls1Δ rad51Δ* strains respectively, and found that D-loops were Rad51-dependent specifically in the *sgs1Δ uls1Δ* strains but not in the *sgs1Δ* strains, following recovery from HU (Figure 4C-E). As HU is a ribonucleotide reductase inhibitor, which reduces the pool of dNTPs necessary to complete replication, D-loops should be able to form following fork cleavage, but only minimal DNA synthesis should be able to occur initially. Only during recovery from HU should substantial DNA replication occur, and thus, we suspect it is during recovery that the effect of Rad51 becomes fully apparent as an increase in the large arc structures. That *sgs1Δ* mutants can form Rad51-independent D-loops is consistent with previous reports showing increased rates of BIR in *sgs1Δ* mutants [26, 42]. Intriguingly, and as detailed in

the *Discussion*, deletion of *ULS1* seems to result in a switch of repair pathway choice, channeling repair of rDNA away from a Rad51-independent pathway into a Rad51-dependent pathway.

Suppression of aberrant rDNA recombination by *ULS1* deletion occurs upstream of HR pathway choice

A reliance on Rad51-dependent D-loops in the absence of Uls1 might seem contradictory to the previous demonstration that deletion of *ULS1* reduces apparent recombination rates in the rDNA in *sgs1Δ* mutants [29]. However, such rates were measured by loss of a marker inserted into one of the tandem rDNA repeats, which reflects recombination errors and not necessarily overall HR efficiency, thus leaving open the possibility that *ULS1* deletion enhances error-free HR repair. At the rDNA, reduced rates of marker loss could be explained by four different mechanisms: 1) reduction in breaks within the rDNA, allowing fewer opportunities for recombination, 2) promotion of non-homologous end joining (NHEJ) to repair a break rather than HR pathways that could otherwise lead to marker loss by crossover events, 3) promotion of non-crossover pathways following formation of a dHJ (e.g. *via* STR-mediated dissolution), or 4) promotion of error-free HR pathways over error-prone ones. Our observation that *sgs1Δ uls1Δ* mutants have more breaks within the rDNA than *sgs1Δ* eliminates the first possibility (Figure 3E-3F). The rescue of *sgs1Δ* mutants by deletion of *ULS1* has been shown to require HR [29], and we also confirm here that this rescue is independent of NHEJ machinery Lig4, Yku70, and Yku80 (Figure 5A), eliminating option 2. To determine whether deletion of *ULS1* could affect recombination rates in *sgs1Δ* mutants following dHJ formation, we implemented a crossover assay utilizing an *ADE2* cassette harboring a site-specific DSB; homology exists on either side of the break and thus repair by GC dominates with dHJs as intermediates ([13, 33]; Supplemental

Figure 4A). In this assay, deletion of *ULS1* did not alter crossover rates in *sgs1Δ* mutants (Figure 5B). Furthermore, in a system in which a DSB was introduced into the *MATa* locus by an inducible HO and GC could be followed over time, *sgs1Δ* and *sgs1Δ uls1Δ* mutants again had no significant difference in crossover rates and also had similar rates of repair (Figure 5C, Supplemental Figure 4B-D) [16]. That deletion of *ULS1* has no effect on DSB-induced crossover rates following dHJ formation, and actually leads to more DSBs specifically at the rDNA RFB, supports the fourth option: that reduced rDNA marker loss results from the promotion of specific error-free HR pathways operating at one-ended breaks arising during DNA replication.

Rescue of *sgs1Δ* by deletion of *ULS1* requires Mms21 SUMO ligase activity

Uls1 is thought to have STUbL activity [43], and so we hypothesized that it might normally function by targeting ubiquitinated proteins for proteasomal degradation during DNA repair. Thus, in the absence of Uls1, a subset of DNA repair proteins might persist and provide benefit to cells lacking Sgs1. And if so, removal of the SUMO ligase responsible for the relevant modification should abrogate any benefit from deletion of *ULS1*. *S. cerevisiae* has only three SUMO ligases, Mms21, Siz1, and Siz2, and so we determined whether any were required for rescue of *sgs1Δ* mutants in the absence of Uls1. *mms21Δ* mutants are inviable, but *mms21*-sp mutants lack a functional SUMO ligase domain and grow at normal rates on rich media. We found that deletion of *ULS1* was unable to confer damage tolerance to *sgs1Δ mms21*-sp mutants on HU and MMS, and *uls1Δ mms21-sp* mutants were synthetically sick on rich media (Figure 6 and Supplemental Figure 5). This interaction was specific to Mms21 among SUMO ligases, as deletion of *SIZ1* or SIZ2 did not abrogate rescue of *sgs1Δ* mutants by *ULS1* deletion (Figure 6). In addition to being a SUMO ligase, Mms21 is part of the Smc5/6 complex, which has important

roles in DNA replication and repair and has close interactions with the STR complex [35, 44-46]. Recently, Mms21 was shown to sumoylate Top3 [35, 45], and thus these observations raise the possibility that such sumoylation might assist Top3 in providing rescue to *sgs1Δ* mutants in the absence of Uls1, although other targets of Mms21 are likely involved.

Discussion

Although roles for Top3 downstream of recombination intermediate formation are well documented, the mechanisms by which Top3 can act prior to recombination intermediate formation are not fully understood. Evidence that Top3 has roles in replication includes elevation in its levels during S-phase, and intra S-phase checkpoint defects in *top3* mutants [47, 48]. Furthermore, Top3 has known Sgs1-dependent functions that could influence replication-associated HR repair prior to recombination intermediate formation, including stabilizing polymerases at stalled replication forks and stimulating 5'-3' end resection at DNA breaks; whether it can function without Sgs1 at these or other early steps is not known [22, 24, 25]. Here, we provide novel evidence supporting a Sgs1-independent role for Top3 in fork processing and restart. Our results suggest that in the absence of Sgs1 and Uls1, Top3 enhances the induction of site-specific breaks and D-loop formation at the rDNA RFB to restart stalled replication forks. Restart of HU-induced fork stalling apparently occurs primarily through a break-induced D-loop intermediate, and not *via* a fork reversal mechanism. Importantly, deletion of *ULS1* alters the genetic requirements for this D-loop formation, resulting in a shift from Rad51-independent D-loops in *sgs1Δ* mutants toward Rad51-dependent D-loops in *sgs1Δ uls1Δ* mutants.

How then, might this repair pathway shift confer resistance to HU in *sgs1* mutants? In the absence of Sgs1, forks become compromised (possibly as a consequence of replisome destabilization) and collapse, resulting in a break of one strand or, as depicted, both the leading and lagging strand templates (Figure 7A-B) [49]. Repair of the lagging strand template could occur through SSA (Figure 7C-D), while the leading strand could reinvade *via* BIR (Figure E-F). Both of these processes can lead to sequence losses, including a loss of repeats within the rDNA, with BIR becoming particularly problematic in the context of HU, as more ssDNA is available, allowing for more opportunities for Rad51-independent strand annealing, and thus potential loss of repeats. In contrast, deletion of *ULS1* leads (directly or indirectly) to stabilization of replication forks, particularly at the rDNA RFB. We propose that Top3 aids in this stabilization by rewinding exposed ssDNA (*i.e.* using its strand passage activity to reanneal strands), preventing aberrant fork collapse (Figure 7G-K). In this context we hypothesize that rewound forks can be cleaved specifically at the RFB to allow for fork restart (Figure 7L). The structure specific endonuclease Mus81-Mms4 is a likely candidate for this role as *uls1Δ mus81Δ* double mutants have known synergistic sensitivity to DNA damaging agents and a delay in S-phase completion following MMS-induced damage [28]. Furthermore, Mus81-Mms4 has been shown *in vitro* to cleave fork structures in such a way as to leave a 5' flap on the leading strand template, and a single strand gap on the lagging strand template, a discontinuity that could potentially favor a GC fork restart event over BIR [50, 51]. Following cleavage by Mus81-Mms4 (or an alternative endonuclease), Rad51-mediated GC can initiate to restart the fork (Figure 7M-N). The distinction between GC and BIR is an important one, as BIR can not only lead to loss of repeats, but can also trigger extensive template switching leading to increased mutagenesis, particularly when Rad51-independent [52-54]. Furthermore, the shift from a

Rad51-independent repair pathway to a Rad51-dependent pathway is also important as Rad51 has been shown to displace Rad52-RPA filaments from ssDNA, a function that would like inhibit SSA events [55]. Consequently, deletion of *ULS1* in *sgs1Δ* mutants results in a switch from an error-prone HR fork restart pathway to a relatively error-free one. Interestingly, initiation of DNA synthesis following BIR is significantly delayed compared to synthesis following GC (4 hrs vs 30 min) [42], and we speculate that this difference could account for the observed delay in recovery from HU-induced filamentous growth in *sgs1Δ vs. sgs1Δ uls1Δ* mutants (Figure 2B). Thus, deletion of *ULS1* could be providing benefit to *sgs1Δ* mutants *via* two means: 1) by accelerating the onset of DNA synthesis following acute damage, and 2) by inhibiting mutagenic DNA synthesis during chronic exposure to HU. This idea that Uls1 acts a DNA repair pathway switch is supported by a recent study by Kramarz, K. *et al.* (2017), which provides evidence for Uls1 indirectly influencing pathway choice via regulation of Srs2 sumoylation [56, 57]. Finally, based on observations showing a lack of X-structure accumulation in *sgs1Δ* mutants exposed to HU, we hypothesize that most fork restart events get channeled through a synthesis dependent strand annealing pathway (SDSA) (Figure 7O-P) rather than through formation and resolution of a dHJ intermediate. Interestingly, similar to what we observed for Top3, rescue of *sgs1Δ* mutants on HU by Srs2 overexpression was only evident in the absence of Uls1 and was dependent on Srs2 being sumoylated [58]. Srs2 is known to promote SDSA by dissolving D-loops in a manner dependent on SUMO and PCNA, and thus our model agrees nicely with recently published data [16, 59, 60]. In the future, it will be interesting to address how Top3 aids in this process, including whether it can indeed diminish levels of ssDNA at a replication fork or if it cooperates with Mus81-Mms4 or some other endonuclease in fork processing.

Top3 can also be sumoylated in an Mms21-specific manner [35, 45]. Uls1 has previously been shown to prevent aberrant SUMO-chain building on the telomere binding protein, Rap1 and the topoisomerase Top2 [61, 62], and thus Top3 might become also hypersumoylated in the absence of Uls1 which might facilitate its role during HR-mediated fork restart. Curiously, Top3 sumoylation has been reported to be dependent on the presence of Sgs1, but whether the loss of apparent sumoylated Top3 seen in *sgs1Δ* mutants is due to an actual inability of Top3 be sumoylated by Mms21, or whether it might instead result from a rapid turnover of sumoylated Top3 *via* Uls1-dependent ubiquitination and proteosomal degradation, has not been explored, leaving open the possibility that sumoylated Top3 could accumulate in *sgs1Δ uls1Δ* mutants [35]. That sumoylation of Top3 might be required specifically for its fork restart activity and not for recombination intermediate resolution is particularly intriguing because overexpression of Top3 in the presence of Uls1, while previously shown to provide rescue to *sgs1Δ* mutants on MMS *via* Rec-X resolution, is not able to confer any resistance to *sgs1Δ* mutants on HU, where stalled forks are the primary lesion ([7, 13] and data presented here). Consistent with these observations, deleting *ULS1* does allow Top3 to provide rescue to *sgs1Δ* mutants on HU, but only has a modest effect in the context of MMS. HU and MMS are often viewed as having similar effects on DNA replication, and although they both can lead to stalled forks and single strand gaps as detected by EM, different repair pathways clearly dominate in response to each. This is most evident *via* 2DGE-SB analyses in *sgs1Δ* mutants, which clearly show that MMS induces Rec-X mediated repair, while HU induces repair *via* fork restart ([3, 4, 7, 12, 13] and data presented here). These observations suggest two different context-specific roles for Top3 in DNA repair: sumoylation-independent functions involving Rec-X resolution, and sumoylation-dependent functions involving replication fork restart.

These findings provide new insight into a mechanism regulating repair pathway choice to restart stalled forks, and suggest a novel role for Top3, independent of its complex members, in mediating DNA repair at a stalled fork, though it is also possible that Sgs1 and Rmi1 could aid in this process. While the data presented here focus on events at the rDNA locus, it is possible that these processes are occurring genome wide, though not immediately evident in our assays. Indeed, events at the rDNA RFB may be particularly easy to detect because it creates a natural concentration of stalled events leading to D-loops at a defined location. The resulting break at this location allowed us to visualize apparent D-loop-based fork restart events by 2DGE-SB, which to our knowledge has not been reported previously. This system should be useful for further investigating the factors and mechanisms that govern repair pathway choices at damaged replication forks.

Figure Legends

Figure 1: Rescue of *sgs1Δ* mutants by deletion of *ULS1* is dependent on Top3. Spot assays comparing the effects of MMS and/or HU on growth of (**A)** WT, *uls1Δ, sgs1Δ, sgs1Δ uls1Δ, sgs1Δ top3Δ, sgs1Δ top3Δ uls1Δ, sgs1Δ rmi1Δ, and sgs1Δ rmi1Δ uls1Δ* mutants, (**B**) *sgs1Δ top3Δ* and *sgs1Δ top3Δ uls1Δ* cells with plasmids overexpressing Top3, catalytically inactive Top3-Y356F or vector control, and (**C**) *sgs1Δ,* and *sgs1Δ uls1Δ* cells with plasmid overexpressing Top3 or vector control. Note that the wild type and mutant Top3 proteins were shown previously to accumulate to similar levels [13].

Figure 2: Deletion of *ULS1* accelerates recovery following HU-induced damage in *sgs1Δ* mutants. (**A**) Quantification of the proportion of cells with filamentous morphology in *sgs1Δ,*

sgs1Δ uls1Δ, sgs1Δ top3Δ, and *sgs1Δ top3Δ uls1Δ* mutants following 12 hours of recovery from 200 mM HU treatment. 407 (*sgs1Δ),* 922 (*sgs1Δ uls1Δ),* 360 (*sgs1Δ top3Δ*), and 625 (*sgs1Δ top3Δ uls1Δ*) cells were counted for each genotype. ***p*-value ≤0.01; calculated using Fisher's exact test. Error bars represent 95% confidence intervals. (**B**) Quantification of the percentage of aberrant cells in *sgs1Δ, sgs1Δ uls1Δ, sgs1Δ top3Δ,* and *sgs1Δ top3Δ uls1Δ* mutants over time. (**C**) Quantification of cell accumulation over time for the genotypes listed in (**B**). Cells in a cluster were counted as one cell. Graphs in (**B**) & (**C**) show mean ± standard deviation. One-way ANOVAs were used to determine statistical significance; *n*=3; ***p*-value ≤0.01, ****p-value* ≤0.001. (D) Quantification of the percentage of cells that form colonies in *sgs1Δ, sgs1Δ uls1Δ, sgs1Δ top3Δ,* and *sgs1Δ top3Δ uls1Δ* mutants following 1 hr HU, 6 hr recovery, and 3 days growth on YPAD. Two-tailed unpaired t-tests were used to determine statistical significance. Graphs represent mean ± S.E.M; *n*=3; **p*-value ≤0.01.

Figure 3: Deletion of *ULS1* in *sgs1Δ* mutants increases species with 2DGE mobility similar to large forks, and in a manner dependent on Top3. (**A**) (*Left*) schematic depicting locations of X-structures, large and small replication forks, and the RFB. (*Right*) Representative 2DGE-SB examining replication intermediates that accumulate in *sgs1Δ, sgs1Δ uls1Δ,* and *sgs1Δ top3Δ uls1Δ* mutants, 1 hour after start of HU treatment and 2 hrs following release from HU. Data for an rDNA fragment containing the RFB is shown. (**B**) Quantification of the sum of the large arc and RFB relative to small arc. Graphs represent mean ± S.E.M.; *n*=2. Two-tailed Student's t-test.. (**C-D**) (*Left*) Representative 2DGE-SB examining replication intermediates following psoralen crosslinking *in vivo* prior to DNA extraction in (**C**) *sgs1Δ* and *sgs1Δ uls1Δ* mutants and (**D**) *sgs1Δ uls1Δ and sgs1Δ uls1Δ top3Δ* mutants exposed to 200 mM HU for 1 hour. (*Right*) Quantification of the sum of the large arc and RFB relative to small arc. Two-tailed Student's t-

test. Graphs represent mean± S.E.M.; n=5, *p-value ≤ 0.05, **p-value ≤ 0.01. (**E**) (*Top*) schematic depicting RFB in relation to sites of restriction enzyme digest and *in vivo* break site. (*Bottom*) one dimensional gel-SB examining breaks at the rDNA replication fork block in WT and *sgs1Δ, sgs1Δ uls1Δ,* and *sgs1Δ top3Δ uls1Δ* mutants. (**F**) Quantification of (**E**): Broken fragments (2.3 Kb) were normalized by dividing over the intact locus fragment (4.6 Kb). Graphs represent mean ± S.E.M.; n=2.

Figure 4: Structures running within large arc and RFB spot are Rad51-dependent D-loops. (**A**) (*Top*) Schematic of replication intermediates following 2DGE-SB under untreated (*control*) and branch migration conditions (+*BM*) following the first dimension (see *Experimental Procedures*). (*Bottom*) representative 2DGE-SB data showing replication intermediates in *sgs1Δ* and *sgs1Δ uls1Δ* mutants untreated (*left column*), or branch migrated in the absence (*middle column*) or presence of Mg^{2+} (*right column*). (**B**) Schematics of 2DGE mobilities of normal replication intermediates (species *i*, *ii*, and *iii*) and those formed by D-loops, without or with branch migration *in vitro*. (*Top*) intermediates formed *in vivo* (*i.e.* without branch migration *in vitro*). D-loops form via breakage of a fork at the RFB, invasion of the truncated chromatid into the intact sister chromatid, and followed by extension by some degree of DNA synthesis (species *iv* and *v*). (*Bottom*) Branch migration of initial D-loops in one direction (to the right in the figure) returns the intermediates to the intact and truncated chromatids formed by the break (species *vii* and *viii*, corresponding to spots *b* and *c*), whereas migration of D-loops that have been extended by new DNA synthesis yield a population of products extending up to full length (species *ix*, corresponding to the line from spot *c* to *a*; note that some of spot *a* presumably also corresponds to fully-replicated X-spike species that have branch migrated into separate products). Branch migration of the variably extended molecules in the other direction, generates bulkier products

that run in a cone above and to the left of the replication arc (species *vi*). (**C**) Representative 2DGE-SB examining replication intermediates in *sgs1Δ, sgs1Δ rad51Δ, sgs1Δ uls1Δ* and *sgs1Δ uls1Δ rad51Δ* mutants exposed to 200 mM HU for 1 hour and following 45 minutes after release from HU. An rDNA fragment containing the replication fork block is shown. (**D-E**) Quantification of C. Graphs represent mean ± S.E.M; *n*=4. Two-tailed Student's t-test; ****p*-value ≤ 0.001.

Figure 5: Deletion of *ULS1* does not affect crossover rates during break repair in *sgs1Δ* mutants. (**A**) Spot assay comparing the effects of HU on growth of *sgs1Δ, sgs1Δ uls1Δ, sgs1Δ lig4Δ, sgs1Δ lig4Δ uls1Δ, sgs1Δ yku70Δ, sgs1Δ yku70Δ uls1Δ, sgs1Δ yku80Δ,* and *sgs1Δ yku80Δ uls1Δ*. (**B**) Quantification of *ADE2* crossover assay. *sgs1Δ* and *sgs1Δ uls1Δ* mutants were transformed with a HpaI digested *ADE2* cassette (Supplemental Figure 4A) and ratios of crossovers to total are shown on the Y-axis. Graph represents mean ± standard deviation; *n*=4. *P-values* were calculated using two-tailed Student's t-test; *p-value*= 0.7627. (**C**) Quantification of HO-inducible crossover assay. HO endonuclease was induced in *sgs1Δ* and *sgs1Δ uls1Δ* mutants with galactose and ratios of crossovers to total were determined 6 hours after induction (all repair events) and in single colonies following 3 days of growth (viable events). Three independent experiments were performed for calculating crossovers at 6 hours. 152 single colonies from *sgs1Δ* and 149 single colonies from *sgs1Δ uls1Δ* were compared to calculate viable crossover events following repair of the HO inducible DSB (*right*). Fisher exact test; p-value = 0.2622.

Figure 6: Rescue of *sgs1Δ* mutants by deletion of *ULS1* requires SUMO ligase Mms21. Spot assay comparing the effects of MMS and HU on growth of *sgs1Δ, sgs1Δ uls1Δ, siz1Δ sgs1Δ,*

siz1Δ sgs1Δ uls1Δ, siz2Δ sgs1Δ, siz2Δ sgs1Δ uls1Δ, mms21-sp sgs1Δ, and *mms21-sp sgs1Δ uls1Δ* mutants.

Figure 7: Models for the fates of HU-arrested forks in *sgs1Δ* and *sgs1Δ uls1Δ* mutants. (**A-F**) Fork restart in *sgs1Δ* mutants. (**A**) HU induces replisome uncoupling, leading to long stretches of ssDNA at the fork. (**B**) In the absence of Sgs1, forks become unstable, leading to breaks on both template strands, (**C**) followed by limited 5' end resection of the lagging strand, which allows for (**D-E**) recombination of the lagging strand *via* SSA. (**F**) The leading strand can then reinvade the newly repaired lagging strand, *via* BIR to reestablish the fork. (**G-P**) Fork restart in *sgs1Δ uls1Δ* mutants. (**G**) In the absence of Uls1, Top3 recognizes and binds the ssDNA at the fork, and (**H-K**) reduces negative supercoiling at the fork by making transient nicks in one strand and mediating strand passage to rewind the fork. (**L**) This provides an ideal substrate for an endonuclease to cleave the fork, (**M-N**) allowing for Rad51-mediated HR, and (**O-P**) subsequent synthesis dependent strand annealing (or alternatively, Rad51-dependent BIR; see Figure 4) to reestablish the fork.

Supplemental Figure Legends

Supplemental Figure 1: HU induces filamentous growth in *sgs1Δ* mutants. Light microscopy images showing HU-induced filamentous growth in *sgs1Δ, sgs1Δ uls1Δ, sgs1Δ top3Δ,* and *sgs1Δ top3Δ uls1* following 4 hr α-factor arrest (G1), 1 hr in 200mM HU (HU), and recovery after HU removal at indicated time points (1.5 hr post -6 hr post). Arrows point to "G1-doublets".

Supplemental Figure 2: Deletion of *ULS1* does not alter the abundance of X-structures. (A) (*Top*) Schematic of probed locus for rDNA. (*Bottom*) Quantification of X-structures relative to

small arc. Graphs represent mean ± S.E.M.; *n*=2. Two-tailed Student's t-test. (B) (*Top*) Schematic of probed locus for region adjacent to ARS305. (*Bottom*) Representative 2DGE-SB examining replication intermediates at a region adjacent to ARS305 in *sgs1Δ, sgs1Δ uls1Δ,* and *sgs1Δ top3Δ uls1Δ* mutants exposed to 200 mM HU for 1 hour and 2 hrs following recovery. **(C) (***Left***)** Representative 2DGE-SB examining replication intermediates in *sgs1Δ top3Δ* and *sgs1Δ top3Δ uls1Δ* mutants exposed to 200 mM HU for 1 hour, and 45 minutes following release from HU. (*Right***)** Quantification of images to left. Graphs represent mean ± S.E.M.; *n*=2.

Supplemental Figure 3: HU-induced structures, migrating as large forks are biochemically consistent with being D-loops (A) Schematic of reversed fork branch migration in the presence or absence of Mg^{2+}. In the absence of Mg^{2+}, reversed forks will first migrate up into a four-way junction and eventually into linearized products (*bottom* images); however, in the presence of Mg^{2+}, reversed forks will be converted to the immobile antiparallel stacked-X structure, and will not be able to branch migrate into linearized fragments. (**B**) *sgs1Δ* mutants were either untreated or treated with MBN prior to 2DGE-SB analysis.

Supplemental Figure 4: Schematics and Southern blot analysis of crossover assays. (**A**) *ADE2* crossover assay schematic. Cleaved plasmid carrying *URA3* and with partial homology to the *ADE2* locus on either side of the HpaI cut site was transfected into cells. Repair of the plasmid off of the endogenous *ADE2* locus occurs either through a crossover mechanism with the plasmid disrupting the *ADE2* locus, resulting in a red colony (crossover), or by a noncrossover mechanism in which the plasmid is religated to itself resulting in a white colony (noncrossover). Cells were grown on SC-URA plates and the number of red and white colonies were counted. Ratios were taken to determine the proportion of crossovers for each genotype. (**B**) HO-inducible crossover assay schematic. Gal-inducible HO cleaves the *MAT*a locus on

Chromosome V. The broken chromosome is repaired off of the uncleavable *MAT*a (*MAT*a-inc) on Chromosome III. Total rates of different types of repair (crossover *vs* noncrossover) were measured for 6 hrs following HO induction. Individual colonies were genotyped 3 days following HO induction, to determine percentage of viable crossover and noncrossover events. Figure adapted from *Ira, G., et al., 2003.* (**C**) Representative Southern blot of HO-inducible crossover assay quantified in Figure 5C "after 6 hrs". Lanes (from left to right): 0, 1, 1.5, 2, 2.5, 3, 3.5, 4, 5, 6, 7, and 8 hrs after HO induction. (**D**) Representative Southern blot for HO-inducible crossover assay quantified in Figure 5C "single colonies." Each lane represents an individual colony. Lanes where both crossover and noncrossover events are present indicate instances where HO-induction occurred in G2 and one sister chromatid was repaired via noncrossover, while the other was repaired by crossover. CO= crossover, NCO= noncrossover.

Supplemental Figure 5: *mms21-sp uls1Δ* double mutants are synthetically sick. Spot assay comparing the effects of MMS and HU on growth of *siz1Δ, siz1Δ uls1Δ, siz2Δ, siz2Δ uls1Δ, mms21-sp,* and *mms21-sp uls1Δ* mutants.

Table 3.1

YB352	*sgs1Δ::HIS3, MAT a*
YB778	*sgs1Δ::HIS3, uls1Δ::G418^R, MAT a*
YB314	*sgs1Δ::HIS3, top3Δ::CaURA3, MAT a*
YB318	*sgs1Δ::HIS3, uls1Δ::G418^R, top3Δ::CaURA3, MAT a*
YB852	*sgs1Δ::HIS3, rmi1Δ::URA3, MAT a*
YB853	*sgs1Δ::HIS3, uls1Δ::G418^R, rmi1Δ::URA3, MAT a*
YB310	*sgs1Δ::HYG + pAG415-GPD-ccdB*
YB311	*sgs1Δ::HYG + pAG415-GPD-TOP3*
YB557	*sgs1Δ::HYG, uls1Δ::G418^R + pAG415-gpd-ccdB, MAT a*

YB558	*sgs1Δ::HYG, uls1Δ::G418^R + pAG415-gpd-TOP3, MAT a*
YB653	*sgs1Δ::HIS3, bar1Δ::NAT^R, MAT a*
YB621	*uls1Δ::G418, sgs1Δ::HIS3, bar1Δ::NAT^R, MAT a*
TB657	*sgs1Δ::HIS3, top3Δ::CaURA3, bar1Δ::NAT^R, MAT a*
YB633	*sgs1Δ::HIS3, top3Δ::CaURA3, uls1Δ::G418, bar1Δ::NAT^R, MAT a*
YB89	*sgs1::LEU2, bar1:: G418^R, rad51::HYG^R, MAT a*
YB818	*sgs1::LEU2, uls1::URA3, bar1::G418^R, rad51::HYG^R, MAT a*
YB533	*mms21-sp::URA3 cir0, MAT a*
YB534	*mms21-sp::URA3, uls1Δ::HYG^R cir0, MAT a*
YB535	*mms21-sp::URA3, sgs1Δ::HIS3, cir0, MAT a*
YB536	*mms21-sp::URA3, sgs1Δ::HIS3, uls1Δ::HYG, cir0, MAT a*
YB143	*siz1Δ::HYG^R, MAT a*
YB325	*uls1Δ::G418^R, siz1Δ::HYG, MAT a*
YB142	*siz1Δ::HYG^R, sgs1Δ::HIS3, MAT a*
YB323	*sgs1Δ::HIS3, uls1Δ::G418^R, siz1Δ::HYG^R, Mat a*
YB665	*siz2Δ::LEU2, MAT α*
YB667	*siz2Δ::LEU2, uls1Δ::HYG, MAT α*
YB669	*siz2Δ::LEU2, sgs1Δ::HIS3, MAT α*
YB671	*siz2Δ::LEU2, sgs1Δ::HIS3, uls1Δ::HYG^R, Mat α*
YB711	*tgI 354, uls1 Δ:G418, sgs1 Δ:LYS5, JKM 146*
YB713	*tgI 354, sgs1 Δ:LYS5 JKM 146*

Acknowledgements

We'd like to thank members of the Johnson lab for their comments on the manuscript, and assistance in data collection, and Jesse Platt, who performed experiments in earlier versions of this manuscript. This work was supported by National Institutes of Health grants R01 AG021521 and P01 AG031862 (F.B.J.) and by NCI Predoctoral Individual National Research Service Award 1 F31 CA189800-0 (M.R.G.)

Conflict of Interest Statement

The authors declare that there are no conflicts of interest.

BIBLIOGRAPHY

1. Bonner, J.N. and X. Zhao, *Replication-Associated Recombinational Repair: Lessons from Budding Yeast.* Genes (Basel), 2016. **7**(8).
2. Branzei, D. and B. Szakal, *DNA damage tolerance by recombination: Molecular pathways and DNA structures.* DNA Repair (Amst), 2016. **44**: p. 68-75.
3. Sogo, J.M., M. Lopes, and M. Foiani, *Fork reversal and ssDNA accumulation at stalled replication forks owing to checkpoint defects.* Science, 2002. **297**(5581): p. 599-602.
4. Lopes, M., et al., *The DNA replication checkpoint response stabilizes stalled replication forks.* Nature, 2001. **412**(6846): p. 557-61.
5. Cotta-Ramusino, C., et al., *Exo1 processes stalled replication forks and counteracts fork reversal in checkpoint-defective cells.* Mol Cell, 2005. **17**(1): p. 153-9.
6. Katou, Y., et al., *S-phase checkpoint proteins Tof1 and Mrc1 form a stable replication-pausing complex.* Nature, 2003. **424**(6952): p. 1078-83.
7. Petermann, E., et al., *Hydroxyurea-stalled replication forks become progressively inactivated and require two different RAD51-mediated pathways for restart and repair.* Mol Cell, 2010. **37**(4): p. 492-502.
8. Ray Chaudhuri, A., et al., *Topoisomerase I poisoning results in PARP-mediated replication fork reversal.* Nat Struct Mol Biol, 2012. **19**(4): p. 417-23.
9. Zellweger, R., et al., *Rad51-mediated replication fork reversal is a global response to genotoxic treatments in human cells.* J Cell Biol, 2015. **208**(5): p. 563-79.
10. Lopes, M., M. Foiani, and J.M. Sogo, *Multiple mechanisms control chromosome integrity after replication fork uncoupling and restart at irreparable UV lesions.* Mol Cell, 2006. **21**(1): p. 15-27.
11. Fumasoni, M., et al., *Error-free DNA damage tolerance and sister chromatid proximity during DNA replication rely on the Polalpha/Primase/Ctf4 Complex.* Mol Cell, 2015. **57**(5): p. 812-23.
12. Liberi, G., et al., *Rad51-dependent DNA structures accumulate at damaged replication forks in sgs1 mutants defective in the yeast ortholog of BLM RecQ helicase.* Genes Dev, 2005. **19**(3): p. 339-50.
13. Glineburg, M.R., et al., *Resolution by unassisted Top3 points to template switch recombination intermediates during DNA replication.* J Biol Chem, 2013. **288**(46): p. 33193-204.

14. Mankouri, H.W. and I.D. Hickson, *Top3 processes recombination intermediates and modulates checkpoint activity after DNA damage.* Mol Biol Cell, 2006. **17**(10): p. 4473-83.
15. Mankouri, H.W., T.M. Ashton, and I.D. Hickson, *Holliday junction-containing DNA structures persist in cells lacking Sgs1 or Top3 following exposure to DNA damage.* Proc Natl Acad Sci U S A, 2011. **108**(12): p. 4944-9.
16. Ira, G., et al., *Srs2 and Sgs1-Top3 suppress crossovers during double-strand break repair in yeast.* Cell, 2003. **115**(4): p. 401-11.
17. Lee, J., et al., *Evidence that a RecQ helicase slows senescence by resolving recombining telomeres.* PLOS Biology, 2007. **5**(6): p. e160.
18. Cejka, P., et al., *Rmi1 stimulates decatenation of double Holliday junctions during dissolution by Sgs1-Top3.* Nat Struct Mol Biol, 2010. **17**(11): p. 1377-82.
19. Cejka, P., et al., *Decatenation of DNA by the S. cerevisiae Sgs1-Top3-Rmi1 and RPA Complex: A Mechanism for Disentangling Chromosomes.* Mol Cell, 2012. **47**: p. 1-11.
20. Plank, J.L., J. Wu, and T.S. Hsieh, *Topoisomerase IIIalpha and Bloom's helicase can resolve a mobile double Holliday junction substrate through convergent branch migration.* Proc Natl Acad Sci U S A, 2006. **103**(30): p. 11118-23.
21. Cobb, J.A., et al., *DNA polymerase stabilization at stalled replication forks requires Mec1 and the RecQ helicase Sgs1.* Embo J, 2003. **22**(16): p. 4325-36.
22. Bjergbaek, L., et al., *Mechanistically distinct roles for Sgs1p in checkpoint activation and replication fork maintenance.* EMBO J, 2005. **24**(2): p. 405-17.
23. Hegnauer, A.M., et al., *An N-terminal acidic region of Sgs1 interacts with Rpa70 and recruits Rad53 kinase to stalled forks.* EMBO J, 2012. **31**(18): p. 3768-83.
24. Niu, H., et al., *Mechanism of the ATP-dependent DNA end-resection machinery from Saccharomyces cerevisiae.* Nature, 2010. **467**(7311): p. 108-11.
25. Cejka, P., et al., *DNA end resection by Dna2-Sgs1-RPA and its stimulation by Top3-Rmi1 and Mre11-Rad50-Xrs2.* Nature, 2010. **467**(7311): p. 112-6.
26. Marrero, V.A. and L.S. Symington, *Extensive DNA end processing by exo1 and sgs1 inhibits break-induced replication.* PLoS Genet, 2010. **6**(7): p. e1001007.
27. Jain, S., et al., *Sgs1 and Mph1 Helicases Enforce the Recombination Execution Checkpoint During DNA Double-Strand Break Repair in Saccharomyces cerevisiae.* Genetics, 2016. **203**(2): p. 667-75.
28. Cal-Bakowska, M., et al., *The Swi2-Snf2-like protein Uls1 is involved in replication stress response.* Nucleic Acids Res, 2011. **39**(20): p. 8765-77.
29. Kramarz, K., et al., *Swi2/Snf2-like protein Uls1 functions in the Sgs1-dependent pathway of maintenance of rDNA stability and alleviation of replication stress.* DNA Repair (Amst), 2014. **21**: p. 24-35.
30. Liberi, G., et al., *Methods to study replication fork collapse in budding yeast.* Methods Enzymol, 2006. **409**: p. 442-62.
31. Giannattasio, M., et al., *Visualization of recombination-mediated damage bypass by template switching*. Nat Struct Mol Biol, 2014. **21**(10): p. 884-92.
32. Weitao, T., et al., *Dna2 helicase/nuclease causes replicative fork stalling and double-strand breaks in the ribosomal DNA of Saccharomyces cerevisiae.* J Biol Chem, 2003. **278**(25): p. 22513-22.
33. Tay, Y.D., J.M. Sidebotham, and L. Wu, *Mph1 requires mismatch repair-independent and -dependent functions of MutSalpha to regulate crossover formation during homologous recombination repair*. Nucleic Acids Res, 2010. **38**(6): p. 1889-901.
34. Jiang, Y.W. and C.M. Kang, *Induction of S. cerevisiae filamentous differentiation by slowed DNA synthesis involves Mec1, Rad53 and Swe1 checkpoint proteins.* Mol Biol Cell, 2003. **14**(12): p. 5116-24.

35. Bonner, J.N., et al., *Smc5/6 Mediated Sumoylation of the Sgs1-Top3-Rmi1 Complex Promotes Removal of Recombination Intermediates*. Cell Rep, 2016. **16**(2): p. 368-78.
36. Panyutin, I.G. and P. Hsieh, *The kinetics of spontaneous DNA branch migration.* Proc Natl Acad Sci U S A, 1994. **91**(6): p. 2021-5.
37. Lambert, S., et al., *Homologous recombination restarts blocked replication forks at the expense of genome rearrangements by template exchange.* Mol Cell, 2010. **39**(3): p. 346-59.
38. Malkova, A., et al., *RAD51-independent break-induced replication to repair a broken chromosome depends on a distant enhancer site.* Genes Dev, 2001. **15**(9): p. 1055-60.
39. Signon, L., et al., *Genetic requirements for RAD51- and RAD54-independent break-induced replication repair of a chromosomal double-strand break.* Mol Cell Biol, 2001. **21**(6): p. 2048-56.
40. Malkova, A., E.L. Ivanov, and J.E. Haber, *Double-strand break repair in the absence of RAD51 in yeast: a possible role for break-induced DNA replication.* Proc Natl Acad Sci U S A, 1996. **93**(14): p. 7131-6.
41. Fabre, F., et al., *Alternate pathways involving Sgs1/Top3, Mus81/ Mms4, and Srs2 prevent formation of toxic recombination intermediates from single-stranded gaps created by DNA replication.* Proc Natl Acad Sci U S A, 2002. **99**(26): p. 16887-92.
42. Jain, S., et al., *A recombination execution checkpoint regulates the choice of homologous recombination pathway during DNA double-strand break repair.* Genes Dev, 2009. **23**(3): p. 291-303.
43. Tan, W., Z. Wang, and G. Prelich, *Physical and Genetic Interactions Between Uls1 and the Slx5-Slx8 SUMO-Targeted Ubiquitin Ligase.* G3 (Bethesda), 2013.
44. Chavez, A., V. Agrawal, and F.B. Johnson, *Homologous recombination-dependent rescue of deficiency in the structural maintenance of chromosomes (Smc) 5/6 complex.* J Biol Chem, 2011. **286**(7): p. 5119-25.
45. Bermudez-Lopez, M., et al., *Sgs1's roles in DNA end resection, HJ dissolution, and crossover suppression require a two-step SUMO regulation dependent on Smc5/6.* Genes Dev, 2016. **30**(11): p. 1339-56.
46. Sollier, J., et al., *The Saccharomyces cerevisiae Esc2 and Smc5-6 proteins promote sister chromatid junction-mediated intra-S repair.* Mol Biol Cell, 2009. **20**(6): p. 1671-82.
47. Chakraverty, R.K., et al., *Topoisomerase III acts upstream of Rad53p in the S-phase DNA damage checkpoint.* Mol Cell Biol, 2001. **21**(21): p. 7150-62.
48. Oakley, T.J., et al., *Inactivation of homologous recombination suppresses defects in topoisomerase III-deficient mutants.* DNA Repair (Amst), 2002. **1**(6): p. 463-82.
49. Ouyang, K.J., et al., *SUMO modification regulates BLM and RAD51 interaction at damaged replication forks.* PLoS Biol, 2009. **7**(12): p. e1000252.
50. Fricke, W.M., S.A. Bastin-Shanower, and S.J. Brill, *Substrate specificity of the Saccharomyces cerevisiae Mus81-Mms4 endonuclease.* DNA Repair (Amst), 2005. **4**(2): p. 243-51.
51. Whitby, M.C., F. Osman, and J. Dixon, *Cleavage of model replication forks by fission yeast Mus81-Eme1 and budding yeast Mus81-Mms4.* J Biol Chem, 2003. **278**(9): p. 6928-35.
52. Ruiz, J.F., B. Gomez-Gonzalez, and A. Aguilera, *Chromosomal translocations caused by either pol32-dependent or pol32-independent triparental break-induced replication.* Mol Cell Biol, 2009. **29**(20): p. 5441-54.
53. Payen, C., et al., *Segmental duplications arise from Pol32-dependent repair of broken forks through two alternative replication-based mechanisms.* PLoS Genet, 2008. **4**(9): p. e1000175.
54. VanHulle, K., et al., *Inverted DNA repeats channel repair of distant double-strand breaks into chromatid fusions and chromosomal rearrangements.* Mol Cell Biol, 2007. **27**(7): p. 2601-14.
55. Sugiyama, T. and N. Kantake, *Dynamic regulatory interactions of rad51, rad52, and replication protein-a in recombination intermediates.* J Mol Biol, 2009. **390**(1): p. 45-55.

56. Kramarz, K., et al., *DNA Damage Tolerance Pathway Choice Through Uls1 Modulation of Srs2 SUMOylation in Saccharomyces cerevisiae.* Genetics, 2017. **206**(1):513-525.
57. Kolesar, P., et al., *Dual roles of the SUMO-interacting motif in the regulation of Srs2 sumoylation.* Nucleic Acids Res, 2012. **40**(16): p. 7831-43.
58. Kramarz, K., et al., *DNA Damage Tolerance Pathway Choice Through Uls1 Modulation of Srs2 SUMOylation in Saccharomyces cerevisiae.* Genetics, 2017. **206**(1): p. 513-525.
59. Saponaro, M., et al., *Cdk1 targets Srs2 to complete synthesis-dependent strand annealing and to promote recombinational repair.* PLoS Genet, 2010. **6**(2): p. e1000858.
60. Mitchel, K., K. Lehner, and S. Jinks-Robertson, *Heteroduplex DNA position defines the roles of the Sgs1, Srs2, and Mph1 helicases in promoting distinct recombination outcomes.* PLoS Genet, 2013. **9**(3): p. e1003340.
61. Lescasse, R., et al., *End-joining inhibition at telomeres requires the translocase and polySUMO-dependent ubiquitin ligase Uls1.* EMBO J, 2013. **32**(6): p. 805-15.
62. Wei, Y., et al., *SUMO-Targeted DNA Translocase Rrp2 Protects the Genome from Top2-Induced DNA Damage.* Mol Cell, 2017. **66**(5): p. 581-596 e6.

Figure 1

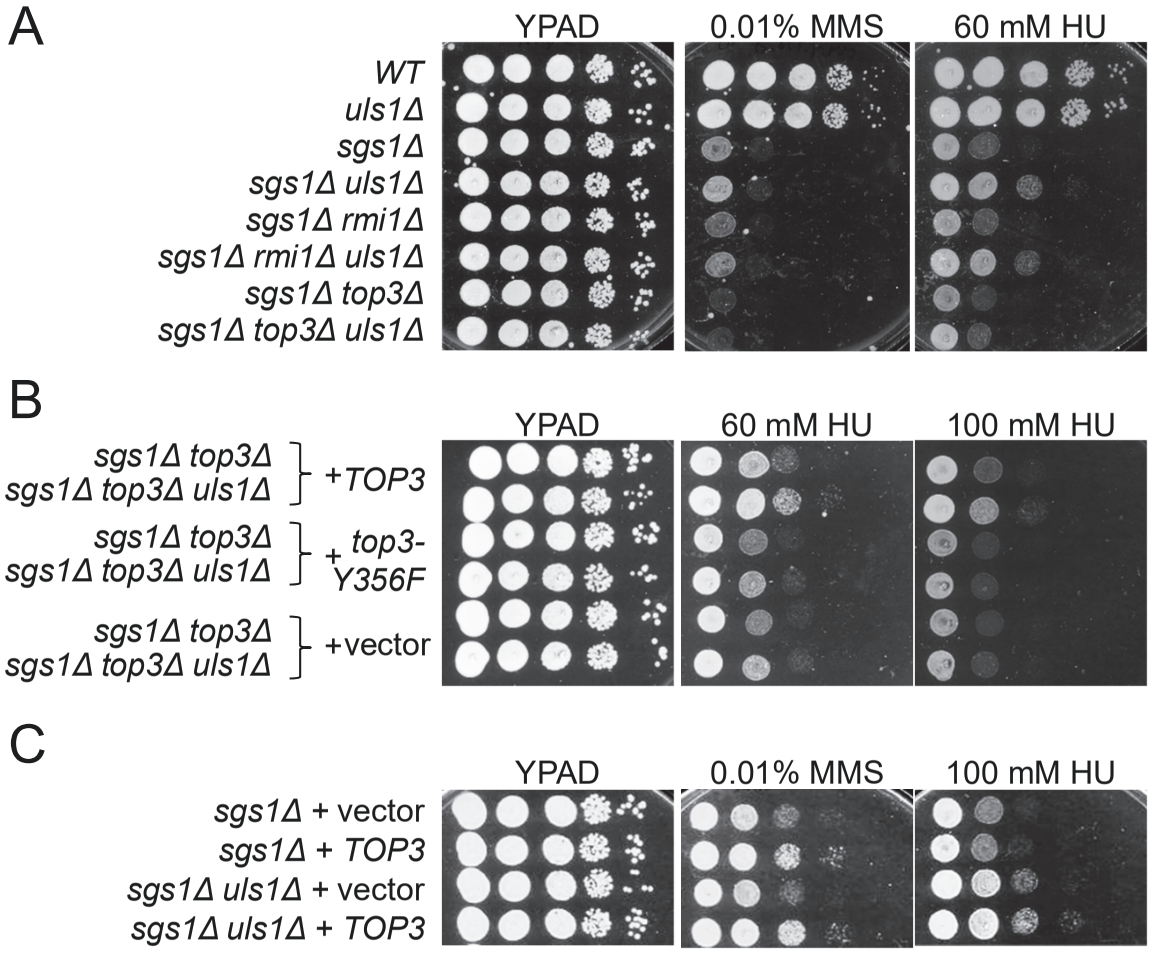
A
YPAD
0.01% MMS
60 mM HU
WT
uls1Δ
sgs1Δ
sgs1Δ uls1Δ
sgs1Δ rmi1Δ
sgs1Δ rmi1Δ uls1Δ
sgs1Δ top3Δ
sgs1Δ top3Δ uls1Δ
B
YPAD
60 mM HU
100 mM HU
sgs1Δ top3Δ
sgs1Δ top3Δ uls1Δ
+TOP3
sgs1Δ top3Δ
sgs1Δ top3Δ uls1Δ
+ top3-Y356F
sgs1Δ top3Δ
sgs1Δ top3Δ uls1Δ
+vector
C
YPAD
0.01% MMS
100 mM HU
sgs1Δ + vector
sgs1Δ + TOP3
sgs1Δ uls1Δ + vector
sgs1Δ uls1Δ + TOP3

Figure 2

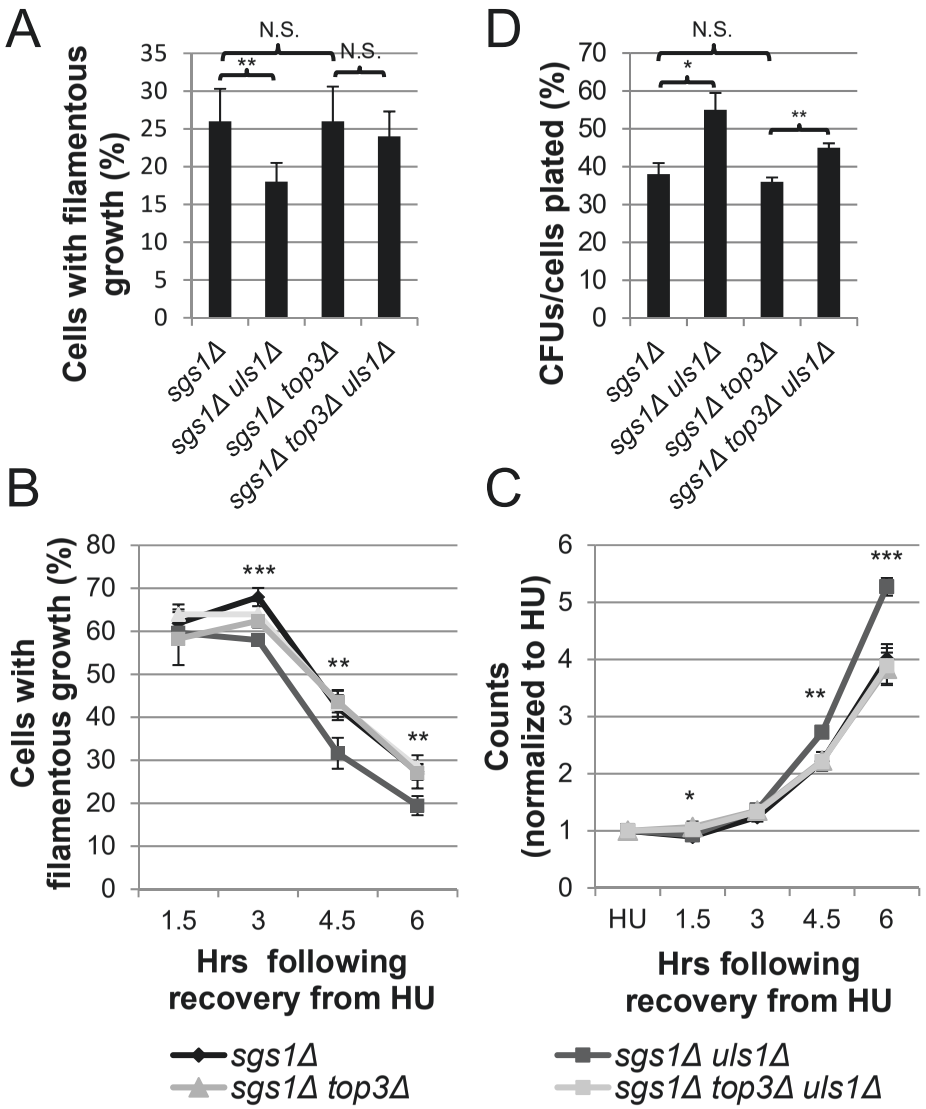
A
N.S.
N.S.
**
Cells with filamentous growth (%)
35
30
25
20
15
10
5
0
sgs1Δ
sgs1Δ uls1Δ
sgs1Δ top3Δ
sgs1Δ top3Δ uls1Δ
D
N.S.
*
**
CFUs/cells plated (%)
70
60
50
40
30
20
10
0
sgs1Δ
sgs1Δ uls1Δ
sgs1Δ top3Δ
sgs1Δ top3Δ uls1Δ
B
Cells with filamentous growth (%)
80
70
60
50
40
30
20
10
0
***
**
**
1.5
3
4.5
6
Hrs following recovery from HU
sgs1Δ
sgs1Δ top3Δ
C
Counts (normalized to HU)
6
5
4
3
2
1
0
***
**
*
HU
1.5
3
4.5
6
Hrs following recovery from HU
sgs1Δ uls1Δ
sgs1Δ top3Δ uls1Δ

Figure 3

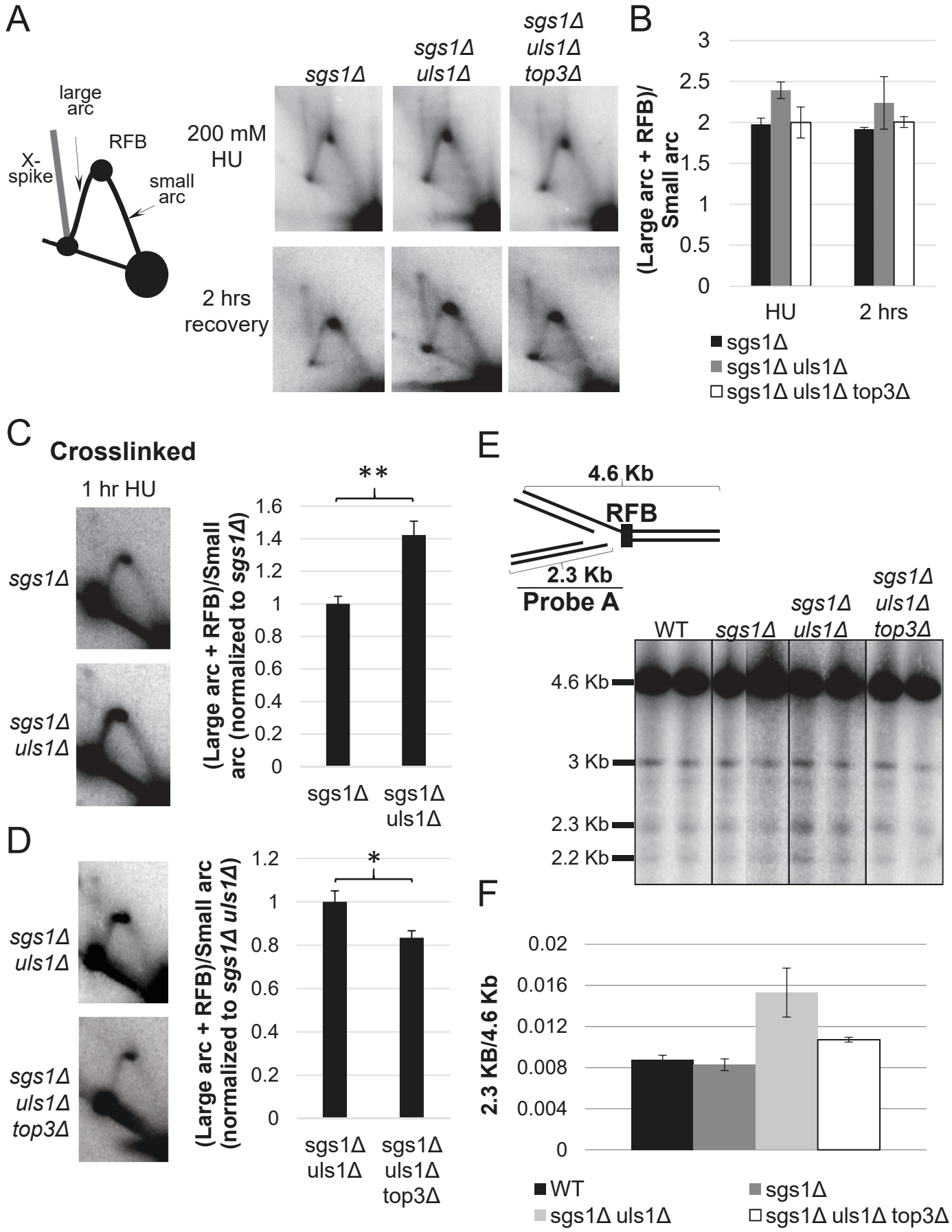
A
large arc
RFB
X-spike
small arc
sgs1Δ
sgs1Δ uls1Δ
sgs1Δ uls1Δ top3Δ
200 mM HU
2 hrs recovery
B
(Large arc + RFB)/ Small arc
HU
2 hrs
sgs1Δ
sgs1Δ uls1Δ
sgs1Δ uls1Δ top3Δ
C
Crosslinked
1 hr HU
sgs1Δ
sgs1Δ uls1Δ
(Large arc + RFB)/Small arc (normalized to sgs1Δ)
**
sgs1Δ
sgs1Δ uls1Δ
D
sgs1Δ uls1Δ
sgs1Δ uls1Δ top3Δ
(Large arc + RFB)/Small arc (normalized to sgs1Δ uls1Δ)
*
sgs1Δ uls1Δ
sgs1Δ uls1Δ top3Δ
E
4.6 Kb
RFB
2.3 Kb
Probe A
WT
sgs1Δ
sgs1Δ uls1Δ
sgs1Δ uls1Δ top3Δ
4.6 Kb
3 Kb
2.3 Kb
2.2 Kb
F
2.3 KB/4.6 Kb
WT
sgs1Δ
sgs1Δ uls1Δ
sgs1Δ uls1Δ top3Δ

Figure 4

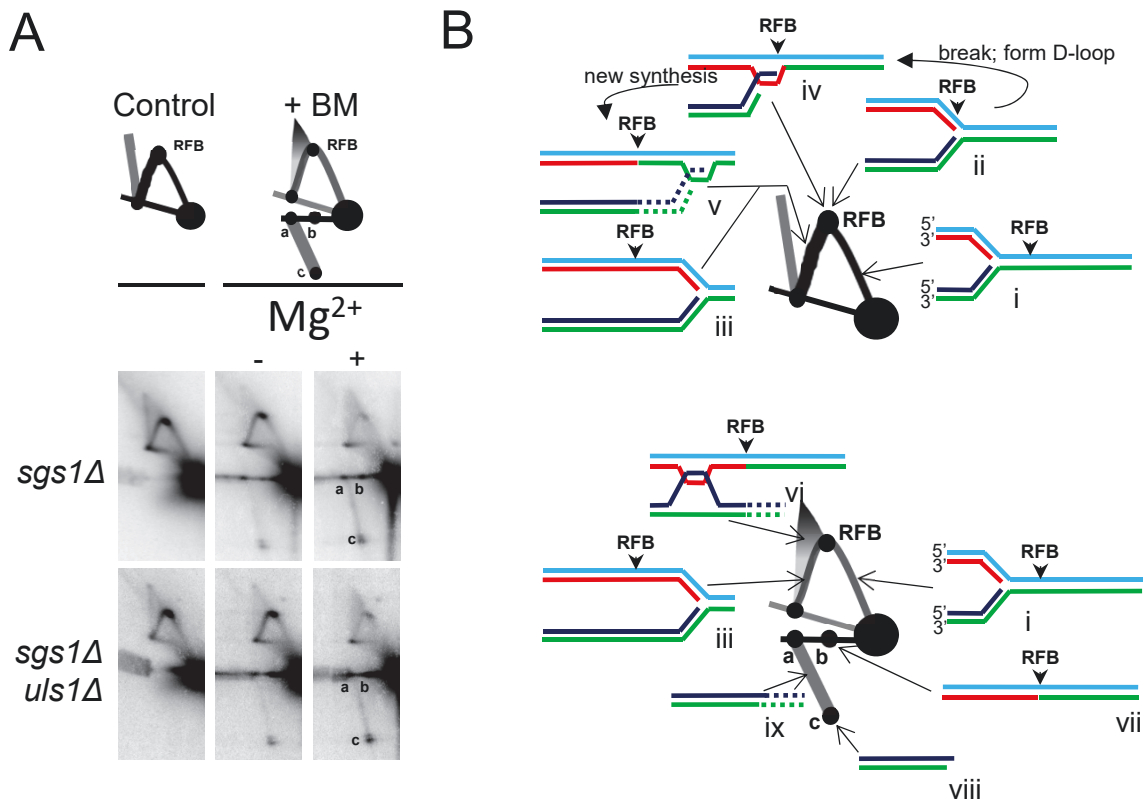
A
Control
+ BM
RFB
a
b
c
Mg2+
-
+
sgs1Δ
sgs1Δ uls1Δ
B
RFB
new synthesis
break; form D-loop
iv
ii
v
i
iii
vi
vii
viii
ix
5'
3'

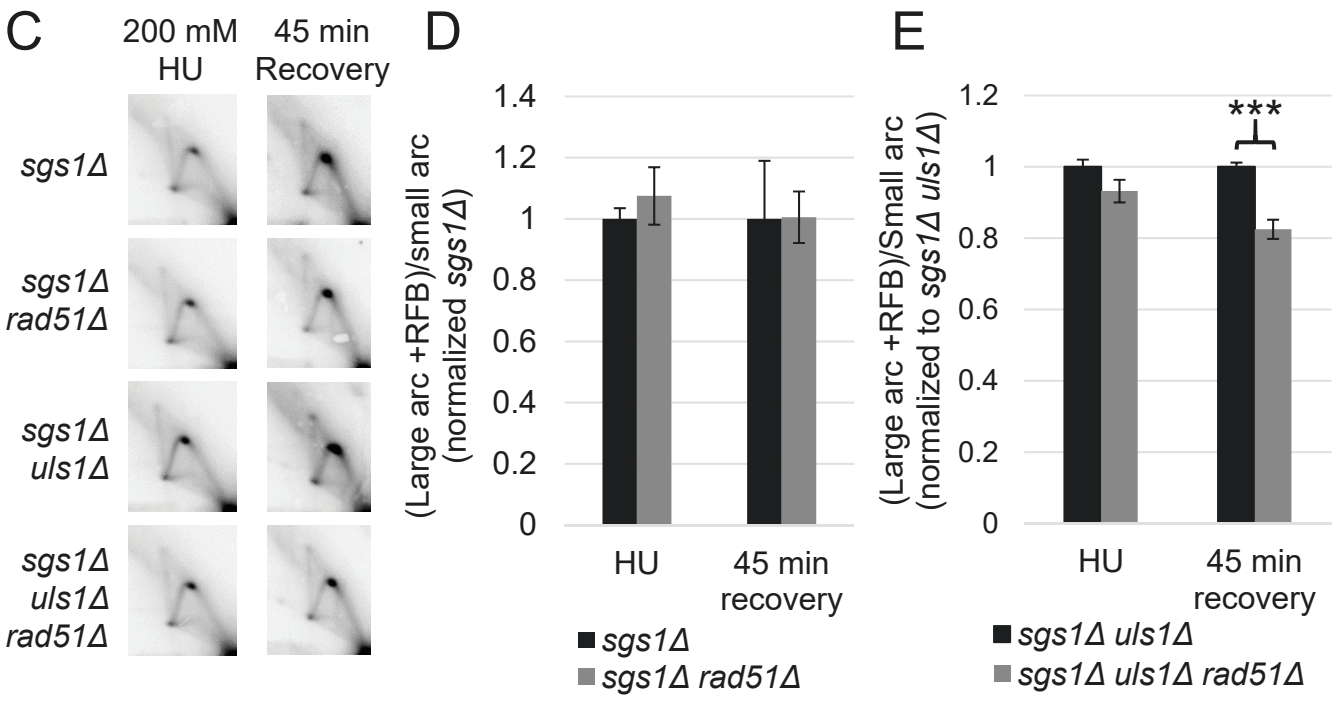
C
200 mM HU
45 min Recovery
sgs1Δ
sgs1Δ rad51Δ
sgs1Δ uls1Δ
sgs1Δ uls1Δ rad51Δ
D
(Large arc +RFB)/small arc (normalized sgs1Δ)
1.4
1.2
1
0.8
0.6
0.4
0.2
0
HU
45 min recovery
sgs1Δ
sgs1Δ rad51Δ
E
(Large arc +RFB)/Small arc (normalized to sgs1Δ uls1Δ)
1.2
1
0.8
0.6
0.4
0.2
0
***
HU
45 min recovery
sgs1Δ uls1Δ
sgs1Δ uls1Δ rad51Δ

Figure 5

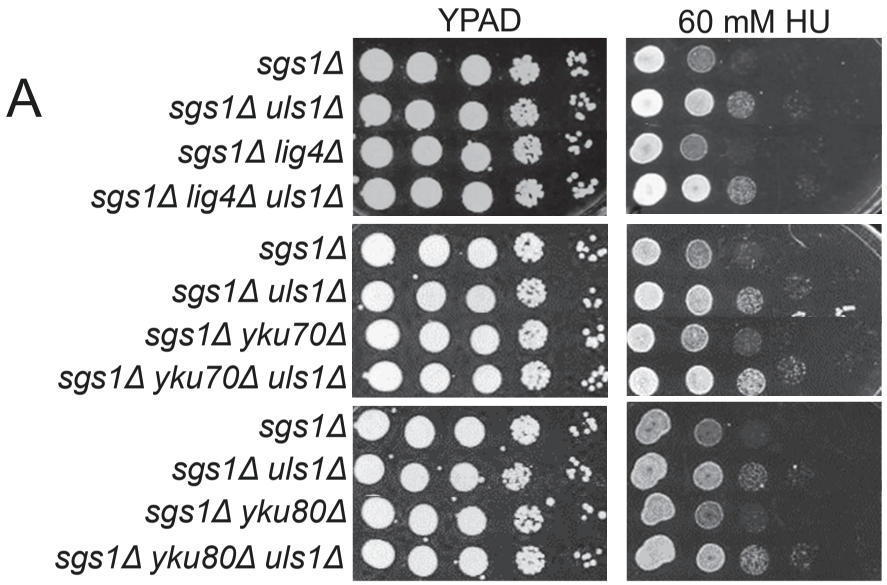
A
YPAD
60 mM HU
sgs1Δ
sgs1Δ uls1Δ
sgs1Δ lig4Δ
sgs1Δ lig4Δ uls1Δ
sgs1Δ
sgs1Δ uls1Δ
sgs1Δ yku70Δ
sgs1Δ yku70Δ uls1Δ
sgs1Δ
sgs1Δ uls1Δ
sgs1Δ yku80Δ
sgs1Δ yku80Δ uls1Δ

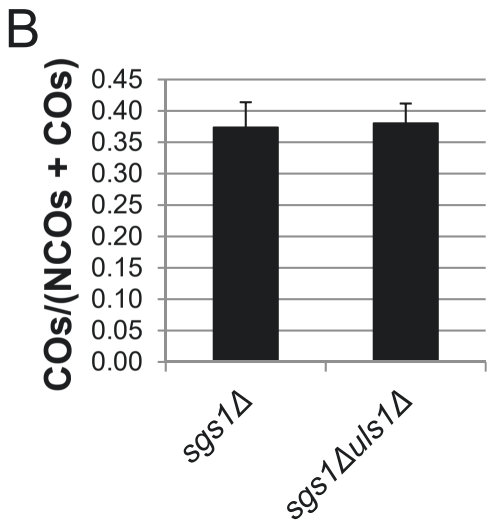
B
COs/(NCOs + COs)
0.45
0.40
0.35
0.30
0.25
0.20
0.15
0.10
0.05
0.00
sgs1Δ
sgs1Δuls1Δ

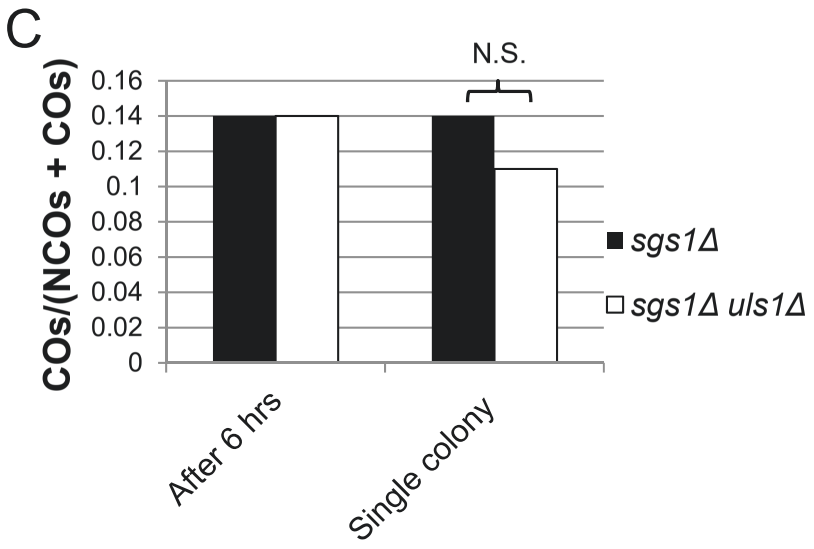
C
N.S.
COs/(NCOs + COs)
0.16
0.14
0.12
0.1
0.08
0.06
0.04
0.02
0
sgs1Δ
sgs1Δ uls1Δ
After 6 hrs
Single colony

Figure 6

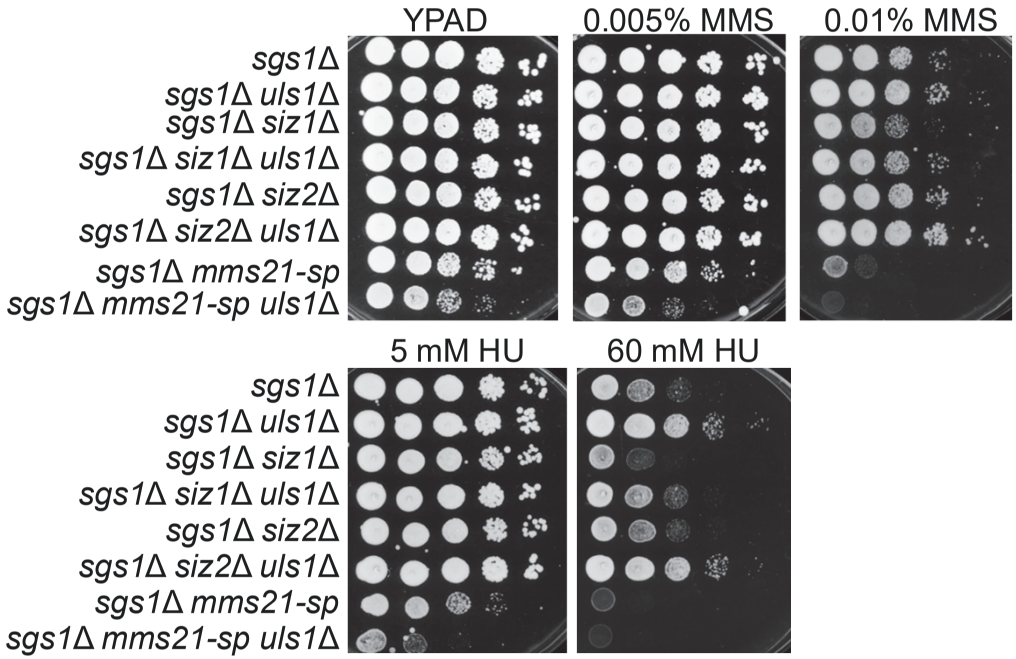
YPAD
0.005% MMS
0.01% MMS
sgs1Δ
sgs1Δ uls1Δ
sgs1Δ siz1Δ
sgs1Δ siz1Δ uls1Δ
sgs1Δ siz2Δ
sgs1Δ siz2Δ uls1Δ
sgs1Δ mms21-sp
sgs1Δ mms21-sp uls1Δ
5 mM HU
60 mM HU
sgs1Δ
sgs1Δ uls1Δ
sgs1Δ siz1Δ
sgs1Δ siz1Δ uls1Δ
sgs1Δ siz2Δ
sgs1Δ siz2Δ uls1Δ
sgs1Δ mms21-sp
sgs1Δ mms21-sp uls1Δ

Figure 7

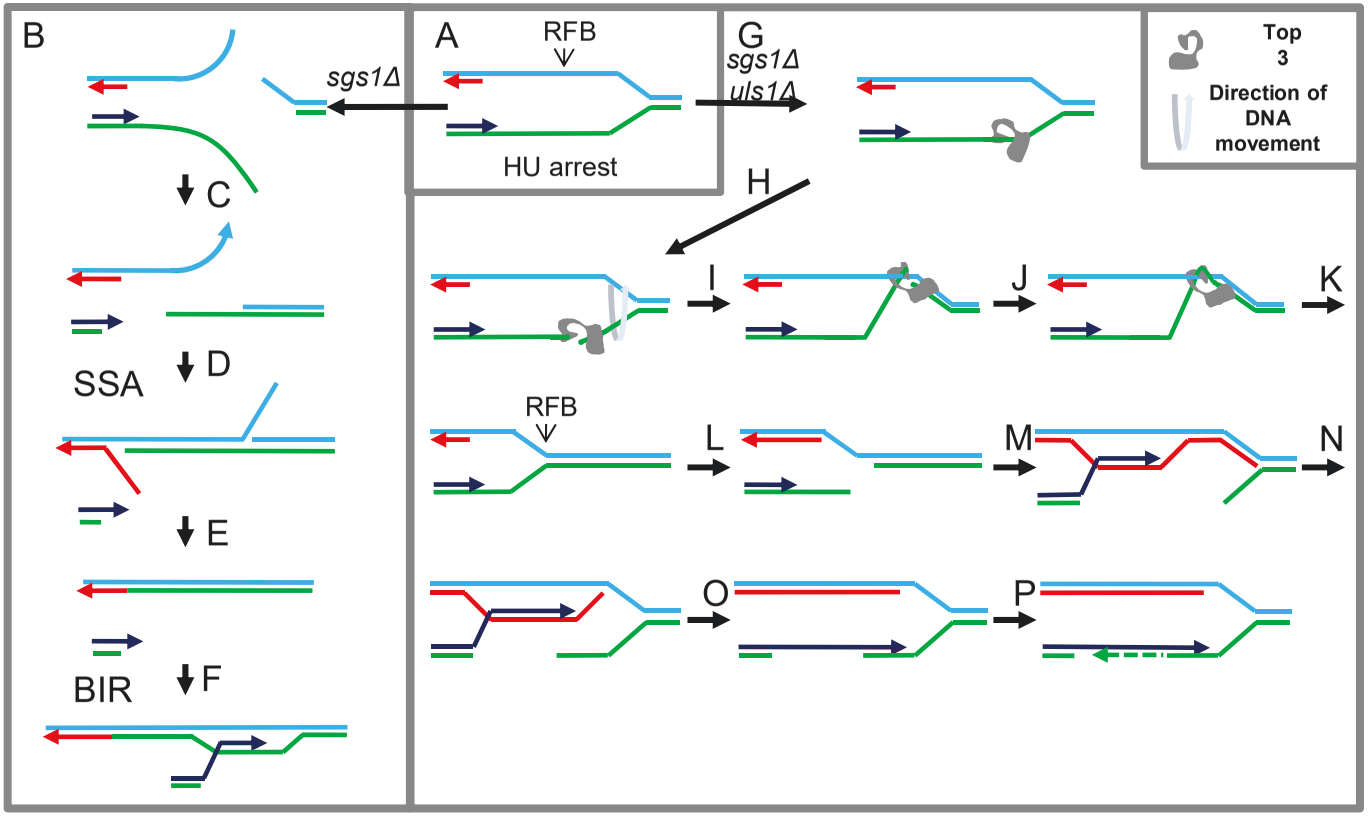
B
sgs1Δ
A
RFB
HU arrest
G
sgs1Δ
uls1Δ
Top 3
Direction of DNA movement
C
H
I
J
K
SSA
D
RFB
L
M
N
E
O
P
BIR
F

Supplemental Figure 1

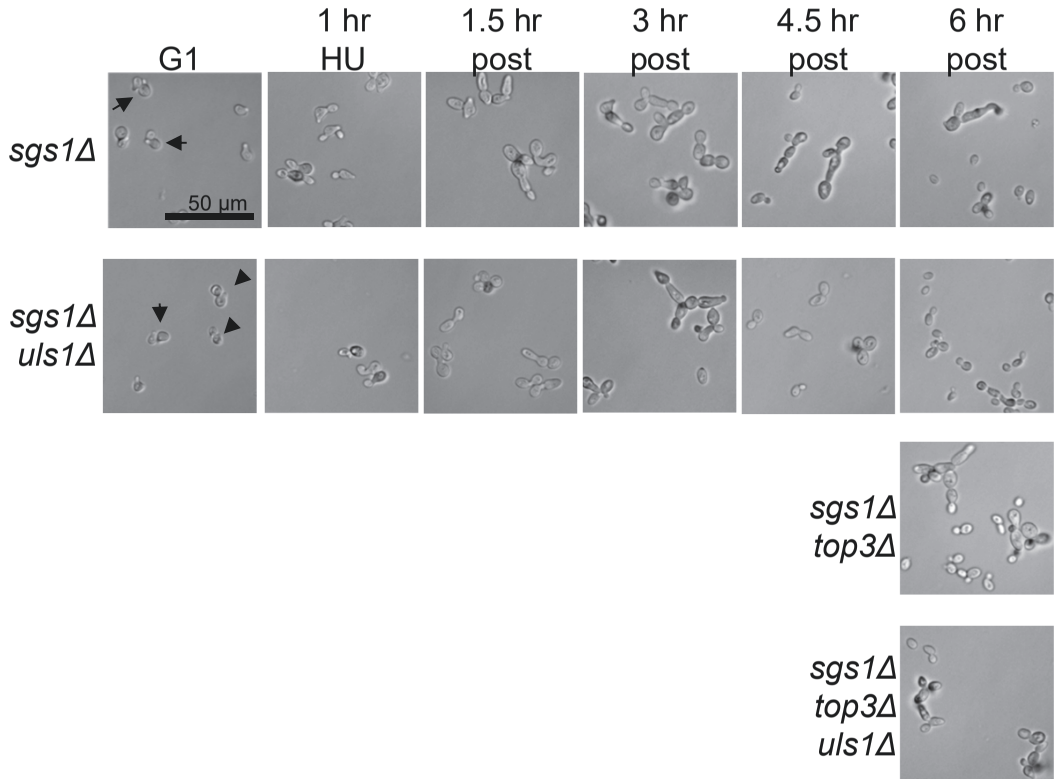

Supplemental Figure 2

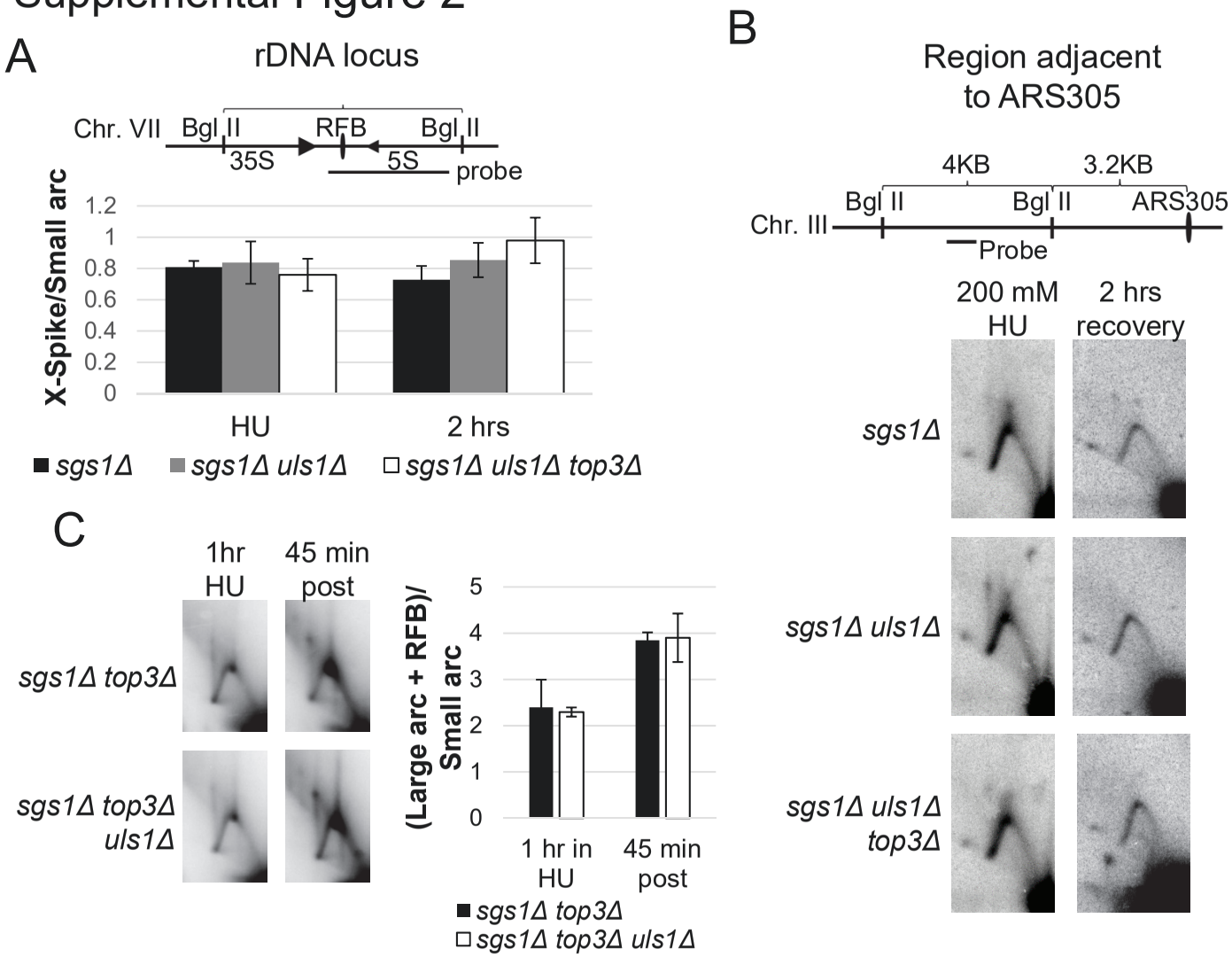

Supplemental Figure 3

A

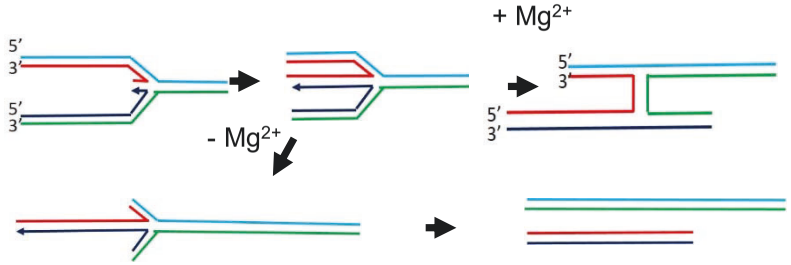

B

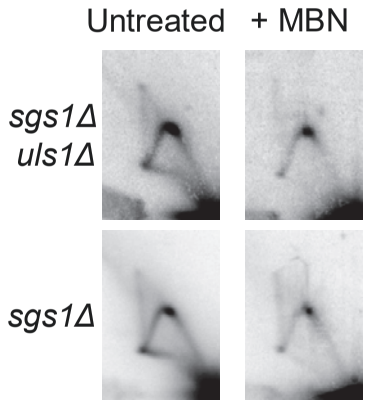

Supplemental Figure 4

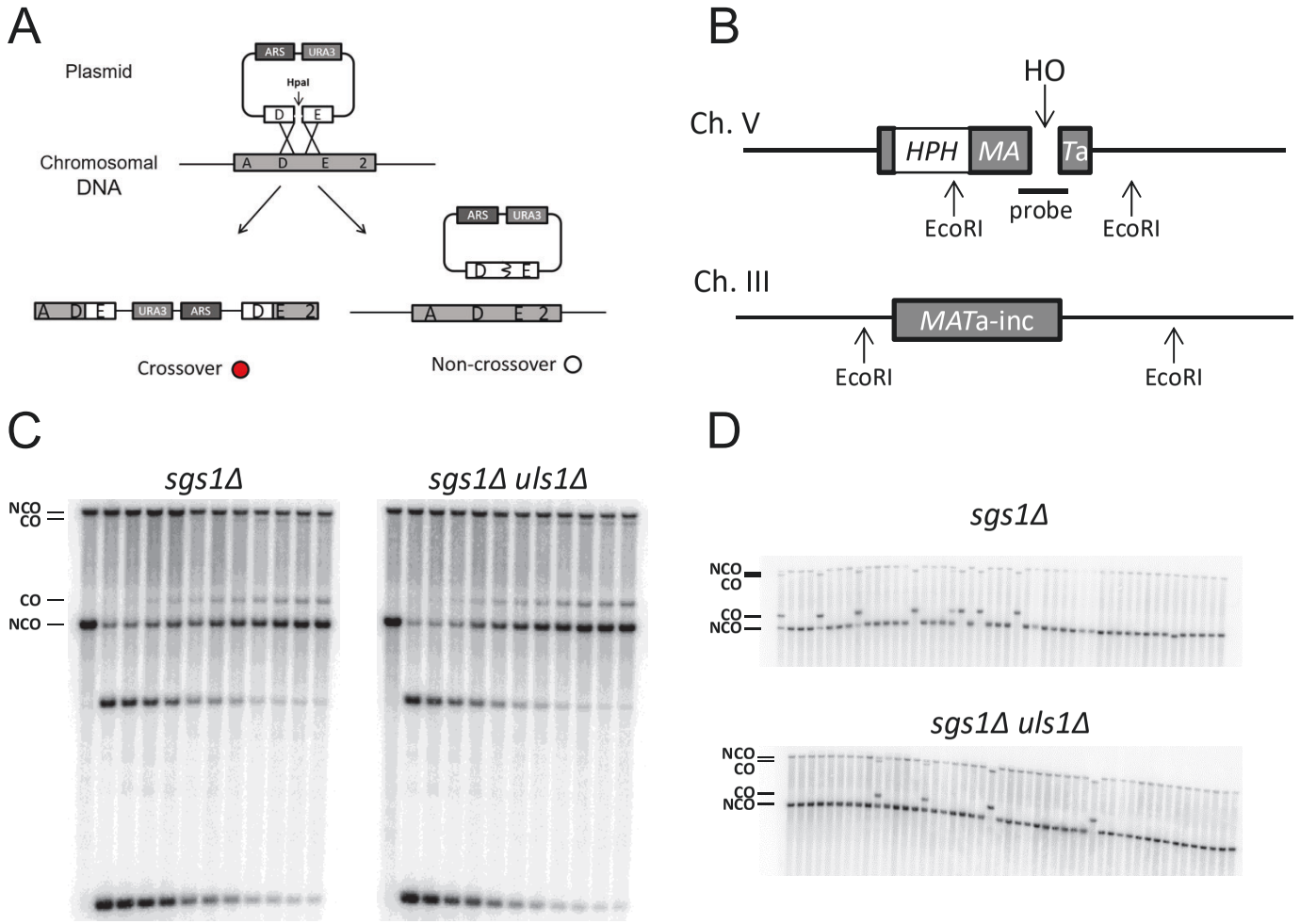

Supplemental Figure 5